Article

Developmental Cell

Tdrd6a Regulates the Aggregation of Buc into Functional Subcellular Compartments that Drive Germ Cell Specification

Graphical Abstract

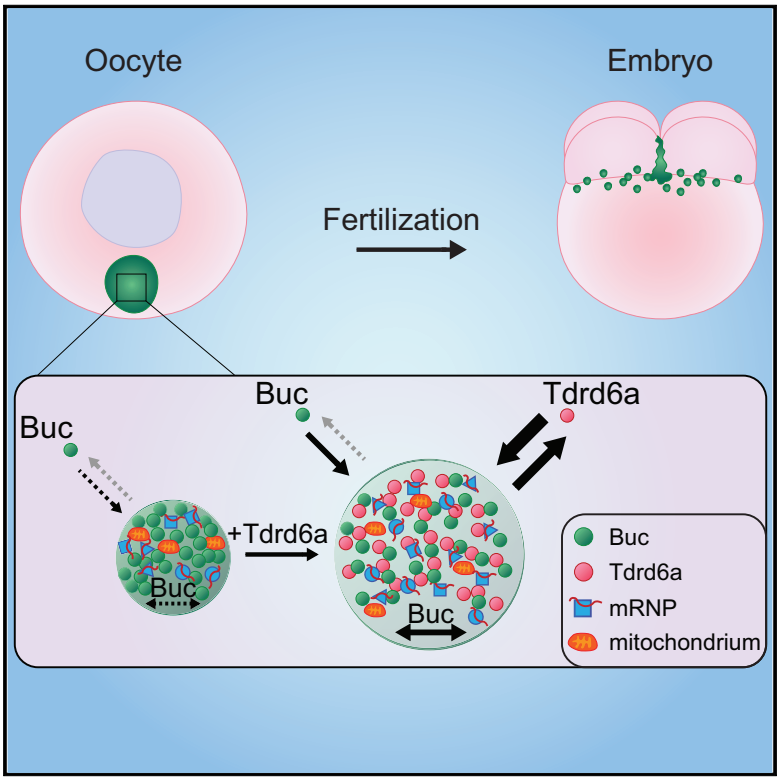

Authors

Elke F. Roovers, Lucas J.T. Kaaij, Stefan Redl, ..., Falk Butter, Alexander van Oudenaarden, René F. Ketting

Correspondence

r.ketting@imb.de

In Brief

Zebrafish Balbiani body and germ plasm are related phase-separated structures. Roovers, Kaaij et al. show that Tdrd6a is required for their formation and mobility through interaction with dimethylated arginines in the prion-like protein Bucky ball, revealing a role for Tudor domain-methylated arginine interactions in *in vivo* phase separation modulation.

Highlights

- Tdrd6a is required for Bucky ball mobility within aggregates, and for PGC formation
- Maternal Tdrd6a coordinates transcript deposition into future PGCs
- A dimethylated tri-RG motif in Bucky ball mediates interaction with Tdrd6a
- The tri-RG motif is essential for Balbiani body and germ cell formation

Roovers et al., 2018, Developmental Cell *46*, 285–301
August 6, 2018
https://doi.org/10.1016/j.devcel.2018.07.009

CellPress

Developmental Cell
Article

Tdrd6a Regulates the Aggregation of Buc into Functional Subcellular Compartments that Drive Germ Cell Specification

Elke F. Roovers,[1,9] Lucas J.T. Kaaij,[1,9] Stefan Redl,[1] Alfred W. Bronkhorst,[1] Kay Wiebrands,[2] António M. de Jesus Domingues,[1] Hsin-Yi Huang,[2] Chung-Ting Han,[3,4] Stephan Riemer,[5] Roland Dosch,[5] Willi Salvenmoser,[6] Dominic Grün,[2,7] Falk Butter,[8] Alexander van Oudenaarden,[2] and René F. Ketting[1,10,*]

[1]Biology of Non-coding RNA Group, Institute of Molecular Biology, Ackermannweg 4, 55128 Mainz, Germany
[2]Hubrecht Institute, Royal Netherlands Academy of Arts and Sciences and University Medical Center Utrecht, Uppsalalaan 8, 3584 CT Utrecht, the Netherlands
[3]Genomics Core Facility, Institute of Molecular Biology, Ackermannweg 4, 55128 Mainz, Germany
[4]CeGaT GmbH, Center for Genomics and Transcriptomics, Paul-Ehrlich-Straße 23, 72076 Tübingen, Germany
[5]Institute of Developmental Biochemistry, Justus-von-Liebig-Weg 11, 37077 Göttingen, Germany
[6]Institute of Zoology, Center of Molecular Bioscience, University of Innsbruck, Technikerstraβe 25, 6020 Innsbruck, Austria
[7]Max Planck Institute of Immunology and Epigenetics, Stübeweg 51, 79108 Freiburg, Germany
[8]Quantitative Proteomics Group, Institute of Molecular Biology, Ackermannweg 4, 55128 Mainz, Germany
[9]These authors contributed equally
[10]Lead Contact
*Correspondence: r.ketting@imb.de
https://doi.org/10.1016/j.devcel.2018.07.009

SUMMARY

Phase separation represents an important form of subcellular compartmentalization. However, relatively little is known about how the formation or disassembly of such compartments is regulated. In zebrafish, the Balbiani body (Bb) and the germ plasm (Gp) are intimately linked phase-separated structures essential for germ cell specification and home to many germ cell-specific mRNAs and proteins. Throughout development, these structures occur as a single large aggregate (Bb), which disperses throughout oogenesis and upon fertilization accumulates again into relatively large assemblies (Gp). Formation of the Bb requires Bucky ball (Buc), a protein with prion-like properties. We found that the multi-tudor domain-containing protein Tdrd6a interacts with Buc, affecting its mobility and aggregation properties. Importantly, lack of this regulatory interaction leads to significant defects in germ cell development. Our work presents insights into how prion-like protein aggregations can be regulated and highlights the biological relevance of such regulatory events.

INTRODUCTION

Phase-separating mechanisms have been acknowledged as important aspects of cell biology. After the initial description of the liquid-like behavior of P granules, peri-nuclear RNA-rich protein aggregates in the *Caenorhabditis elegans* germline and many other RNA-containing granules have been shown to have similar properties (Brangwynne et al., 2009, 2011; Kroschwald et al., 2015). Important players in the formation of these structures are proteins containing intrinsically disordered regions (IDRs) and/or prion-like domains (PrDs) (Kato et al., 2012; Kroschwald et al., 2015). Such proteins have the propensity to self-aggregate and potentially trigger other proteins to phase separate as well (Prusiner, 1998; Shorter and Lindquist, 2005). In many ways, biologically functional protein assemblies such as P granules resemble pathogenic protein-aggregation states. It has been suggested that such disease-causing aggregations are an extreme manifestation of an abundantly used mechanism to form membrane-less compartments (Shin and Brangwynne, 2017). This suggests that mechanisms are in place that prevent healthy, functional aggregates to transform into pathological forms.

In many organisms, germ cell fate is imposed on cells through the cytoplasmic inheritance of P granule-like structures, called germ plasm (Gp) (Ikenishi, 1998; Raz, 2003). In zebrafish, Gp originates from an evolutionary conserved electron-dense aggregate in the oocyte, called the Balbiani body (Bb) (Kloc et al., 2004). The mRNAs enriched in the Bb and Gp are often germline-specific, and in zebrafish, these include *vasa*, *nanos3*, and *dazl* (Hashimoto et al., 2004; Köprunner et al., 2001; Yoon et al., 1997). Depletion of single Gp mRNAs can have detrimental effects on primordial germ cell (PGC) numbers, showing that individual Gp components are important for PGC specification and survival (Köprunner et al., 2001; Slaidina and Lehmann, 2017; Tzung et al., 2015; Weidinger et al., 2003).

Bucky ball (Buc) is a protein known to play a key role in the formation of the Bb in zebrafish (Bontems et al., 2009; Marlow and Mullins, 2008). Overexpression of Buc in zygotes revealed that Buc is sufficient to induce ectopic PGCs, suggesting it is also involved in the formation of the Bb-related Gp structure (Bontems et al., 2009). Buc contains a PrD, and elegant studies on its homolog in *Xenopus* (Xvelo) have demonstrated that these proteins self-aggregate into membrane-less organelles that display amyloid-like features (Boke et al., 2016).

Core Piwi-interacting RNA (piRNA) pathway components, such as Ziwi in zebrafish and Aub in *Drosophila*, are present in the Gp as well (Harris and Macdonald, 2001; Houwing, 2009). Furthermore, it has been shown in *Drosophila* that piRNA pathway components inherited via the Gp are essential for transposon silencing in the offspring (Brennecke et al., 2008), and piRNA-mRNA interactions have been proposed to drive mRNA localization to Gp (Barckmann et al., 2015; Vourekas et al., 2016). Many proteins involved in the piRNA pathway have been identified through genetic and biochemical approaches including multi-Tudor domain-containing proteins (Tdrds) (Siomi et al., 2010). Tdrds play important roles in the formation of nuage, a peri-nuclear protein-RNA aggregate that associates closely with mitochondria. For some Tdrds, it has been shown that they bind to symmetrically dimethylated arginine (sDMA) residues on their interaction partners. In zebrafish, for instance, the interaction between Tdrd1 and the Piwi protein Zili is mediated via a specific sDMA site in Zili (Huang et al., 2011).

One of the Tdrds that has received relatively little attention is Tdrd6, the closest vertebrate homolog to *Drosophila* Tudor (Tud). Tud has been shown to interact with Piwi proteins Aub and Ago3 and plays a role in the localization of Aub to Gp and polar granule formation (Kirino et al., 2010; Nishida et al., 2009; Thomson and Lasko, 2004). In mice, TDRD6 plays a role in establishing the chromatoid body, a testis-specific structure that resembles Gp, and the localization of piRNA pathway components to this body (Vasileva et al., 2009). In addition, it is involved in spliceosome assembly in primary spermatocytes (Akpınar et al., 2017). However, a specific molecular function of Tdrd6 or Tud has thus far not been demonstrated.

We show that Tdrd6a is required for coordinated loading of essential Gp components into PGCs through fine-tuning of the aggregating properties and mobility of the Bb organizer Buc. The Tdrd6a-Buc interaction represents one of the few documented cases that demonstrate how the aggregation of a prion-like protein is regulated *in vivo*. We speculate that similar phase separation-regulating mechanisms may act in other cell types as well.

RESULTS

Tdrd6a Is Gonad Specific and Localizes to Nuage, the Bb, and Gp

The zebrafish genome encodes three Tdrd6 paralogs: *tdrd6a–c*. In this study, we focused on *tdrd6a*. Tdrd6a contains seven Tudor domains and is 2,117 amino acids in length (Figure S1A). Germline-specific expression of *tdrd6a* was validated by RT-PCR (Figure S1B). Immunohistochemistry (IHC) confirmed that Tdrd6a is expressed in the ovary, where it localizes to nuage (Figure 1A, arrowhead) and to the Bb (Figure 1A, arrow). Tdrd6a is also maternally provided and localizes to the Gp in 4-cell stage embryos (Figure 1B, arrowheads). 24 hours post fertilization (hpf), Tdrd6a is restricted to PGCs, where it again localizes to nuage (Figure 1C, arrowheads). We confirmed the identity of the Tdrd6a-containing structures using established markers for the nuage, Bb and the Gp, using both IHC and localization of transgenic Tdrd6a-mCherry (Figure S1C). These results demonstrate that Tdrd6a is maternally contributed and localizes to three conserved and related structures involved in germline specification and maintenance: the Bb, Gp, and nuage.

Identification and Characterization of a *tdrd6a* Mutant Allele

We isolated a *tdrd6a* allele harboring a premature stop codon (Q158X) from an ENU mutagenized library (Wienholds, 2002). Western blot analysis confirmed loss of Tdrd6a in homozygous mutant animals (Figure S1D). *Tdrd6a*$^{-/-}$ oocytes showed complete loss of Tdrd6a staining in peri-nuclear nuage (Figure S1E, arrowhead) and Gp in 4-cell stage embryos (Figure S1F, arrowheads). Some residual staining remained in the Bb in *tdrd6a* mutants (Figure S1E, arrow); however, a strong Tdrd6a-related Bb phenotype (see later) and the presence of a Tdrd6a-mCherry transgene in both nuage and the Bb suggest that this is due to cross reactivity of the antibody in IHC. Homozygous zygotic (Z) and maternal-zygotic (MZ) *tdrd6a* mutants are fertile, indicating that Tdrd6a is not essential for fertility. We conclude that *tdrd6a*^{Q158X} represents a strong loss-of-function allele.

Tdrd6a Does Not Affect piRNAs

Next, we performed a Tdrd6a immunoprecipitation (IP) on ovary lysates, followed by label-free quantitative mass spectrometry (Figure 1D). Besides Tdrd6a, we found strong enrichments for several complexes containing RNA-binding proteins (RBPs), including the Exon Junction Complex (EJC) and the cytoplasmic polyadenylation element binding protein complex (CPEB). In addition, we identified the Piwi pathway components Ziwi, Zili, and Tdrd7. Finally, we found that Buc was highly enriched.

Given the interaction with Ziwi and Zili, we probed for a role of Tdrd6a in the piRNA pathway. We first validated the Tdrd6a interaction with Ziwi and Zili (Figure S2A). Despite these interactions, small RNA (smRNA) sequencing of total ovary did not show significant differences between piRNAs of *tdrd6a*$^{+/-}$ and *tdrd6a*$^{-/-}$ animals (Figures S2B–S2D). We only observed a small but significant reduction in the typical antisense bias for piRNAs mapping to retrotransposons (Figure S2E). When we roughly divided oocytes into early ($\varnothing$ < 300 μm) and later stages ($\varnothing$ > 300 μm), we noticed that this represents a defect in accumulation of antisense piRNAs during early oogenesis only (Figures S2F–S2J). In conclusion, while Tdrd6a associates with Ziwi and Zili, its absence barely affects piRNA populations.

Tdrd6a Affects PGC Formation

MZ *tdrd6a* mutants have a strong tendency to develop into males. Since the amount of PGCs can have an impact on sex determination in zebrafish (Tzung et al., 2015), we examined the effect of Tdrd6a on PGC formation. In both wild-type (wt) and MZ *tdrd6a*$^{-/-}$ embryos, PGCs marked by the *vasa:egfp* transgene (Krøvel and Olsen, 2002) were at the genital ridge at 24 hpf (Figures 1E and 1F, arrowhead). However, we observed a significant reduction in PGC number in the offspring from *tdrd6a*$^{-/-}$ females, irrespective of the genotype of the father (Figure 1G).

Tdrd6a Affects Coordinated Loading of Gp mRNAs into PGCs

To learn more about the underlying cause of the PGC defect, we performed single-cell RNA-sequencing (scRNA-seq) on PGCs

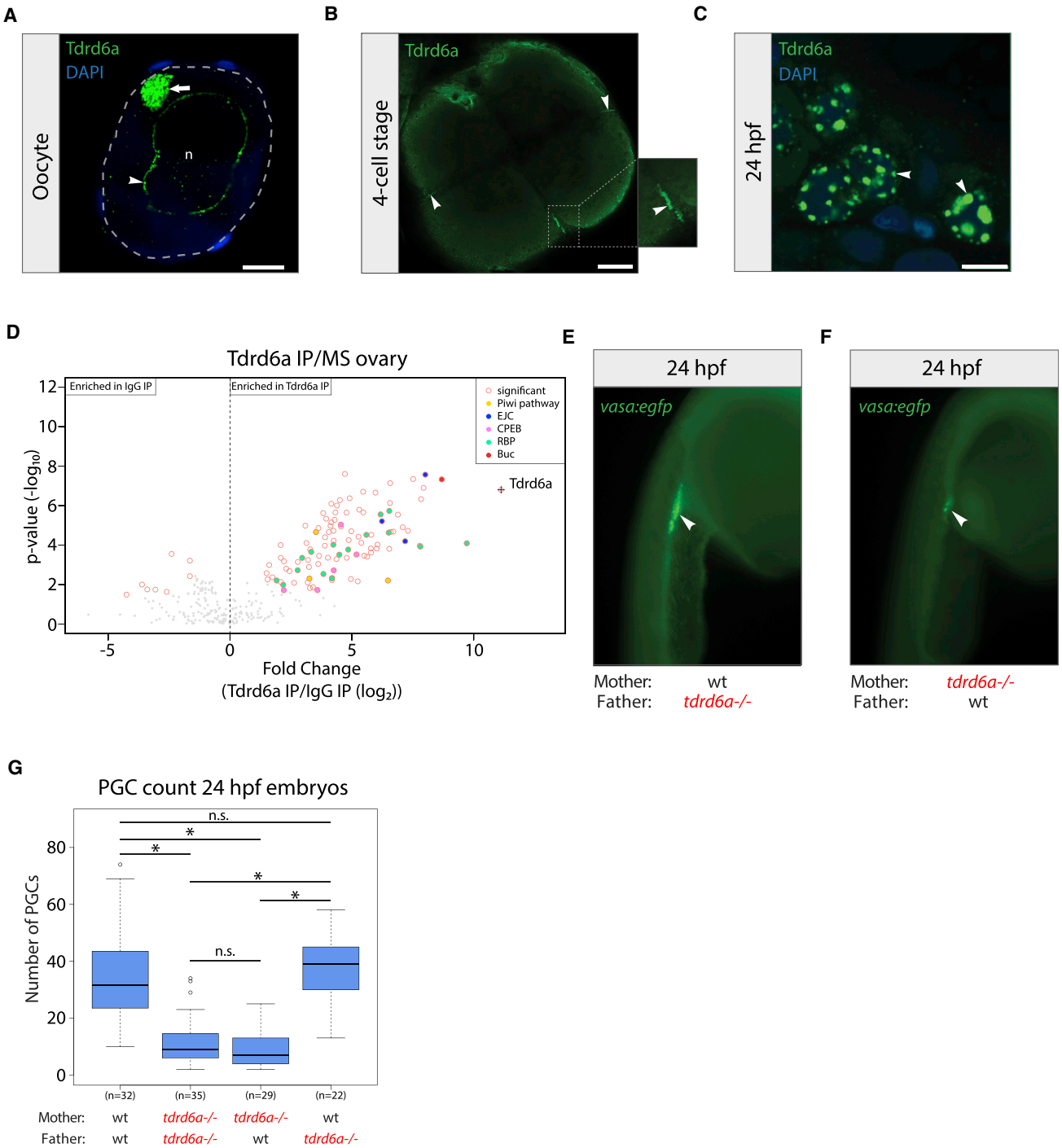

Figure 1. Tdrd6a Is Germline Specific and Required for PGC Formation

(A) IHC for Tdrd6a in oocytes. Arrowhead and arrow indicate Tdrd6a staining in the nuage and Bb, respectively. Gray dashed line outlines the cell, n = nucleus. Scale bar, 10 μm.

(B) IHC for Tdrd6a in 4-cell stage embryos. Arrows indicate Tdrd6a localization to the Gp. Scale bar, 100 μm.

(C) Tdrd6a localizes to peri-nuclear nuage granules (arrowheads) in PGCs at 24 hpf. Scale bar, 7.5 μm.

(D) MS of Tdrd6a IPs on an ovary, compared to IgG (immunoglobulin G) control.

(E and F) 24 hpf embryos derived from wt (E) or *tdrd6a* mutant mothers (F) in a *vasa:egfp* background. Arrowheads indicate the PGCs.

(G) Quantification of PGC numbers in 24 hpf embryos from the crosses indicated on the x axis (* indicates p value < 0.0001, n.s. = non-significant, calculated by Wilcoxon test).

See also Figures S1 and S2.

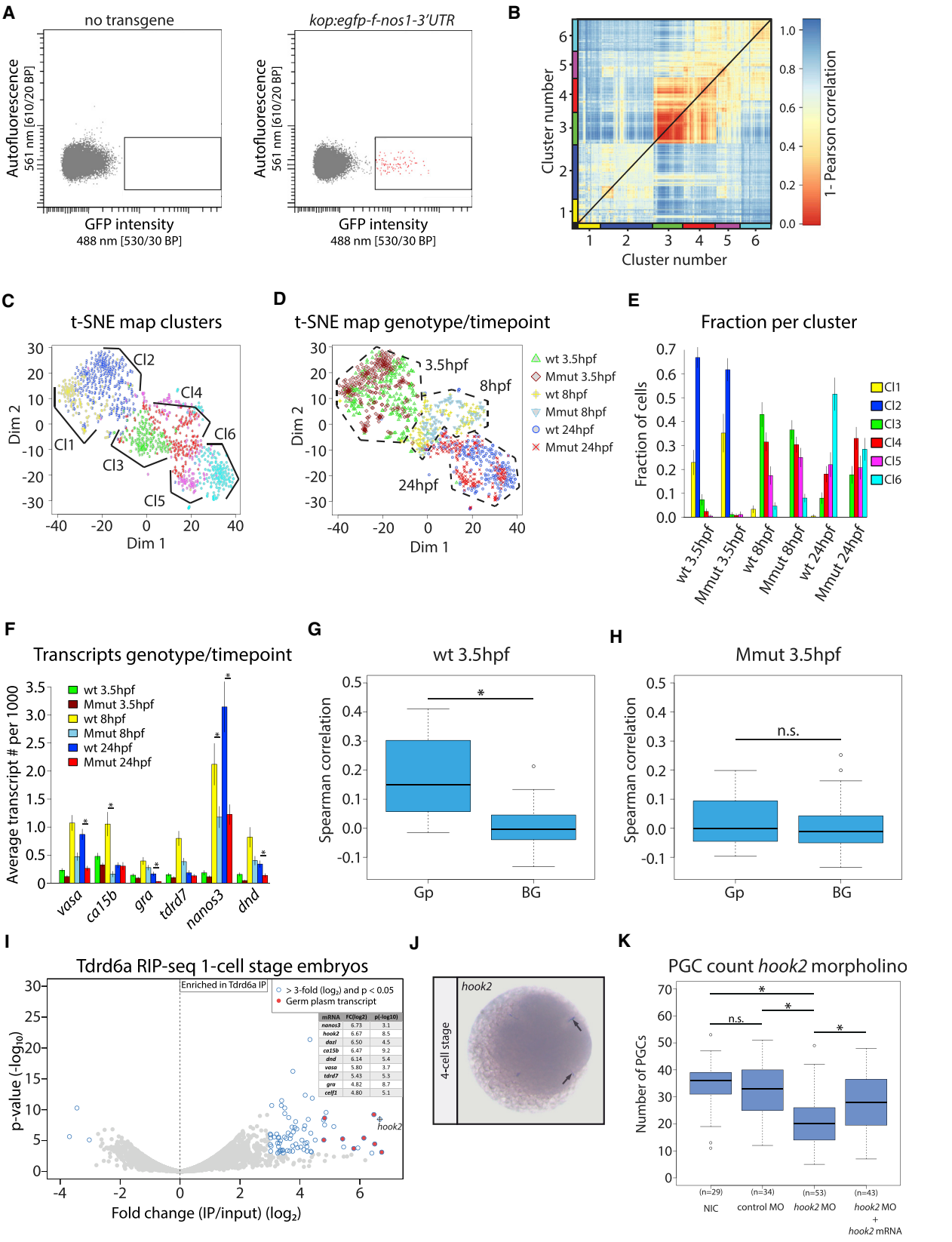

(legend on next page)

isolated from embryos spawned by *tdrd6a*$^{+/-}$ (wt) and *tdrd6a*$^{-/-}$ (Mmut) mothers, both crossed with *tdrd6a*$^{+/+}$ males. PGCs were marked using the *kop:egfp-f-nos1-3′ UTR* transgene (Blaser et al., 2005) and isolated by fluorescence-activated cell sorting (FACS) (Figure 2A). Three time points were analyzed: (1) when PGCs can be first identified using transgenic GFP expression (3.5 hpf), (2) during migration of the PGCs (8 hpf), and (3) when the PGCs have reached the genital ridge (24 hpf).

Roughly 1,100 PGCs were sequenced and analyzed using RaceID2 (Figure S3A) (Grün et al., 2014, 2016; Hashimshony et al., 2012). Representation of the pairwise distances of the single cell transcriptomes in a heatmap revealed two main clusters, which can be further subdivided into clusters 1 and 2 and clusters 3–6 by k-medoids clustering (Figure 2B). Representation of this data in t-distributed stochastic neighbor embedding (t-SNE) maps (Van Der Maaten and Hinton, 2008) revealed that clusters 1 and 2 predominantly harbor 3.5 hpf old PGCs, whereas clusters 3–6 consist of PGCs from 8 hpf and 24 hpf (Figures 2C and 2D). Consistent with this, the pluripotency gene *nanog* is selectively expressed in clusters 1 and 2 (Figure S3B) (Takahashi and Yamanaka, 2006). In contrast, the *rps* gene family, which has been shown to be upregulated after the maternal-to-zygotic transition (MZT) (Siddiqui et al., 2012), is expressed in clusters 3–6 (Figure S3C). No strong differences between genotypes could be observed for 3.5 hpf and 8 hpf PGCs (Figure 2E). However, a significant fraction of 24 hpf Mmut PGCs was enriched in cluster 4 (Figures 2E and S3D), which is dominated by wt PGCs of 8 hpf, suggesting that PGCs lacking maternal Tdrd6a experience developmental delay between 8 hpf and 24 hpf.

Since individual Gp transcripts can influence PGC numbers (Köprunner et al., 2001; Tzung et al., 2015; Weidinger et al., 2003), we tested if PGCs lacking Tdrd6a generally have lower Gp mRNA levels. Of the 8 known zebrafish Gp transcripts (Hashimoto et al., 2004; Köprunner et al., 2001; Strasser et al., 2008; Wang et al., 2013; Weidinger et al., 2003; Yoon et al., 1997), 6 transcripts passed our filtering criteria (see STAR Methods). While at 8 hpf and 24 hpf PGCs lacking Tdrd6a indeed tended to have significantly fewer Gp mRNAs than wt, at 3.5 hpf, no significant difference was found (Figure 2F). In line with this, bulk RNA-seq at the 1-cell stage did not reveal significant effects on mRNA levels (Figures S3E and S3F). Hence, the reduction in PGC number observed upon loss of maternal Tdrd6a most likely is not due to an overall reduction of Gp transcripts provided by the mother.

We then computed all pairwise correlations between the individual Gp mRNAs in wt PGCs at 3.5 hpf and compared these to pairwise correlations of non-Gp background (BG) mRNAs (see STAR Methods). This revealed a general positive correlation for Gp mRNAs in wt PGCs (Figures 2G and S3G), indicating that relatively fixed ratios of individual Gp transcripts are loaded into PGCs. Strikingly, in the absence of Tdrd6a, this positive correlation is completely lost (Figures 2H and S3G). Together, these data show that the stoichiometry of Gp mRNAs in single PGCs is tightly controlled and that this depends on maternally provided Tdrd6a.

Tdrd6a Interacts with Known Gp mRNAs

Since Tdrd6a is required for correct loading of Gp transcripts into PGCs, we next explored whether Tdrd6a interacts with Gp-residing mRNAs through RNA-IP followed by sequencing (RIP-seq). Strikingly, all known Gp mRNAs were strongly enriched in the Tdrd6a RIP-seq compared to input (Figure 2I). We validated these findings using Tdrd6a RIP-qPCR for the Gp markers *vasa, dazl*, and *nanos3*, revealing between a 50- and a 100-fold enrichment in the Tdrd6a RIPs (Figure S3H). The mRNA that was most strongly enriched in the RIP-seq was *hook2* (Figure 2I). *Hook2* is an unknown Gp component in zebrafish but reported to be present in *Xenopus* Gp (Owens et al., 2017). Interestingly, in our scRNA-seq data, *hook2* behaves similar to other Gp markers and also displays the typical Tdrd6a-dependent positive correlation with other Gp transcripts (Figures S3I and S3J). Indeed, in situ hybridization (ISH) confirmed the presence of *hook2* in zebrafish Gp (Figure 2J). Finally, translation inhibition morpholino (MO) injections revealed that *hook2* affects PGC numbers (Figure 2K), substantiating that *hook2* is a bona fide Gp component.

It has been reported that in *Drosophila*, the PIWI protein Aub plays a role in regulating Gp mRNA stability and localization

Figure 2. Single Cell RNA-Seq Analysis Reveals that Maternal Tdrd6a Mediates Positive Correlation of Loading of Gp-Residing mRNAs into PGCs

(A) Flow cytometry plots of the sort strategy used in this study. Representative FACS plots of embryos 8 hpf without or with the *kop:egfp* transgene are shown. Positive events are indicated in red.

(B) Heatmap indicating transcriptome distances of ~1,100 PGCs computed as 1-Pearson's correlation coefficient. K-medoids clustering identified six clusters, which are color coded on the x and y axes.

(C) Similar as in (B) but now visualized in a t-SNE map. Clusters identified by k-medoids clustering are color coded as in (B).

(D) t-SNE map highlighting the genotype and developmental time point of the individual PGCs as indicated.

(E) Barplot displaying the fraction of cells per clusters identified in (B) for the different genotype-developmental time combinations. Error bars were derived from error propagation.

(F) Barplot showing the average transcript counts per 1,000 transcripts per cell of six Gp transcripts in all six different genotype-developmental time point combinations, as indicated. Error bars represent the SEM (* indicates p value < 0.01, calculated by negative binominal statistics and corrected for multiple testing [Benjamini–Hochberg]).

(G and H) Boxplots displaying the Gp-Gp and BG-BG correlations in wt and Mmut embryos, respectively (* indicates p value < 0.001, n.s. = non-significant, calculated by Wilcoxon test).

(I) Volcano plot displaying the fold difference between Tdrd6a RIP-seq and input on the x axis (average of three biological replicates). y axis: p value belonging to the observed differences between Tdrd6a RIP-seq and input. Listed are the values of enriched Gp transcripts.

(J) ISH against *hook2* at the 4-cell stage. Arrows indicate Gp.

(K) Quantification of PGC numbers observed in embryos in morpholino knockdown (MO KD) injection experiment. NIC = non-injected control; the control MO targets the *fus* transcript; the *hook2* mRNA contained mismatches at the *hook2* MO target site and rescues the KD (* indicates p value < 0.01, n.s. = non-significant, calculated by Wilcoxon test).

See also Figure S3.

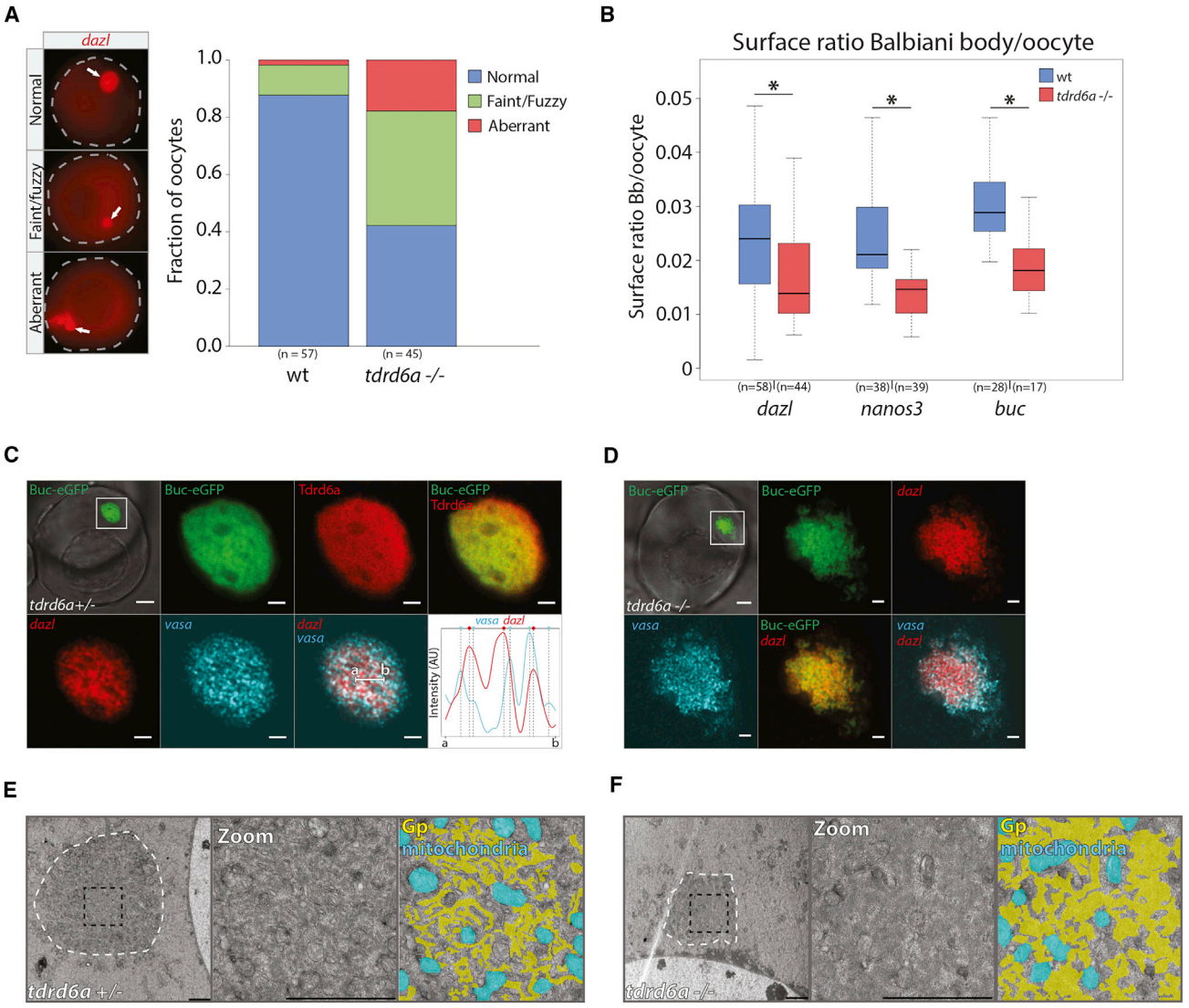

Figure 3. Tdrd6a Is Required for Bb Integrity

(A) Quantification of Bb phenotypes as indicated based on *dazl* FISH on oocytes (examples indicated on the left, arrows indicate Bb).

(B) Surface ratio of Bbs in wt versus *tdrd6a* mutant oocytes (* indicates p value < 0.001, Wilcoxon test).

(C and D) Confocal images of Buc-eGFP-positive oocytes in tdrd6a$^{+/-}$ (C) and *tdrd6a*$^{-/-}$ (D) background. IHC for Tdrd6a and double smFISH was performed and displayed as indicated. *Dazl* and *vasa* signals typically do not overlap, illustrated in the line graph. Intensity for *dazl* (red) and *vasa* (cyan) signals over line a-b (see overlay), with vertical lines indicating fluorescence peaks per smFISH signal (highlighted by colored circle on top) showing transcript peaks are in a separate phase.

(E and F) Electron micrographs of Bbs of *tdrd6a*$^{+/-}$ (E) and *tdrd6a*$^{-/-}$ (F) oocytes (white dashed line). The zoom (black dashed square) is shown with (right) and without (middle) overlays that mark the Gp (yellow) and mitochondria (cyan). Scale bars, 10 μm (overview C and D), 2 μm (zoom) (C and D), and 2 μm (E and F). See also Figure S4.

(Barckmann et al., 2015; Vourekas et al., 2016). In analogy, we performed Ziwi RIP-qPCR experiments on 1-cell stage embryos for *vasa*, *dazl*, and *nanos3*, using the same experimental conditions used for the Tdrd6a RIP-qPCR experiment. The enrichment values for the tested mRNAs were all below 3-fold (Figure S3K), while western blot confirmed that the IPs were successful (Figure S3L). These enrichment values for Ziwi are in sharp contrast to the values obtained in Tdrd6a RIPs, indicating that Ziwi-messenger ribonucleoprotein (mRNP) interactions are not very prominent, or stable in these experiments.

Tdrd6a Affects Bb Organization

We next probed for Bb integrity in the presence and absence of Tdrd6a by doing whole mount fluorescence ISH (FISH) on oocytes against *dazl*. In *tdrd6a* mutant oocytes, the Bb often appears to be smaller relative to the entire oocyte, lacking a well-defined edge or even being further distorted. We quantified these defects by classifying the observed structural abnormalities (Figure 3A) and calculating the size ratio between the Bb and the oocyte using various probes (Figure 3B).

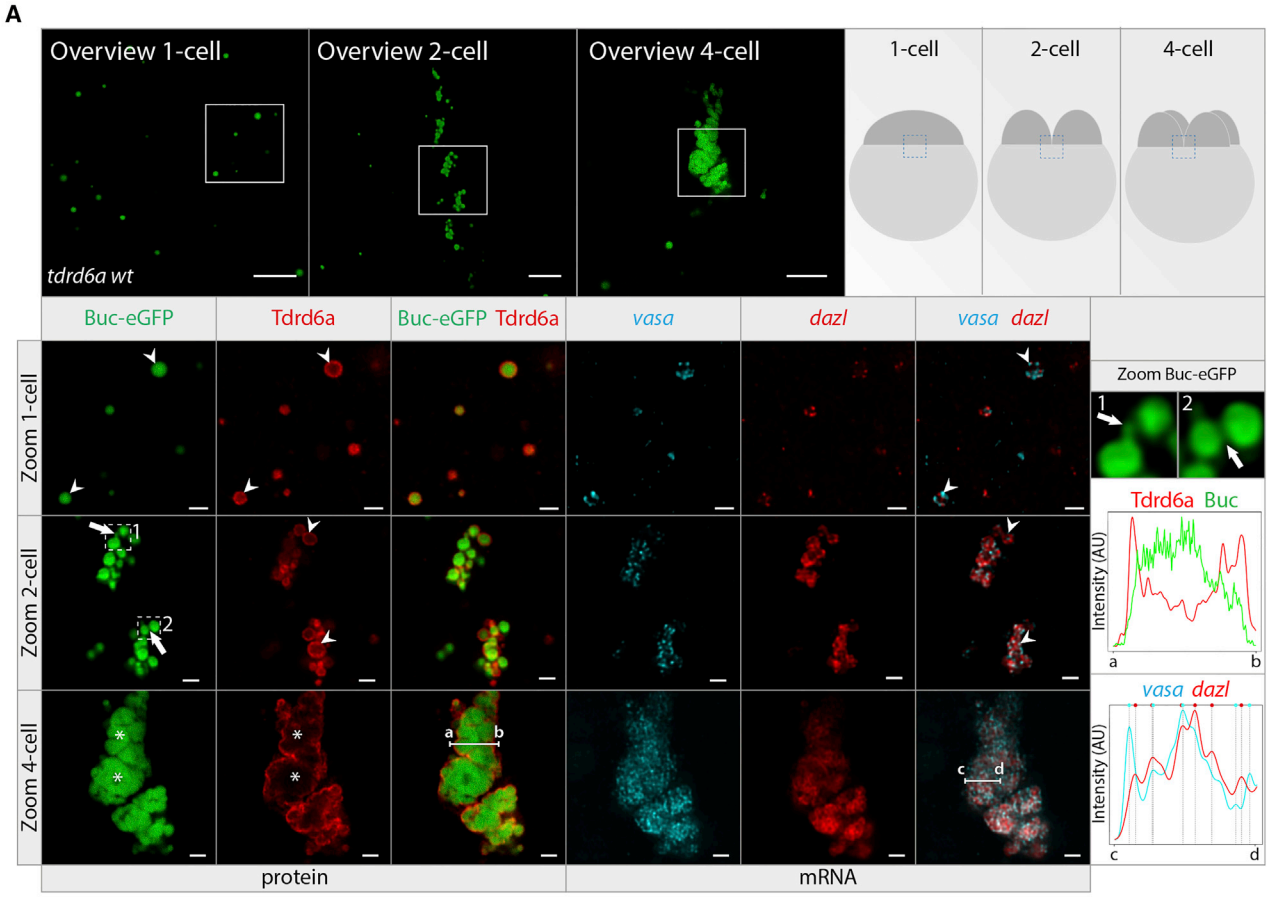

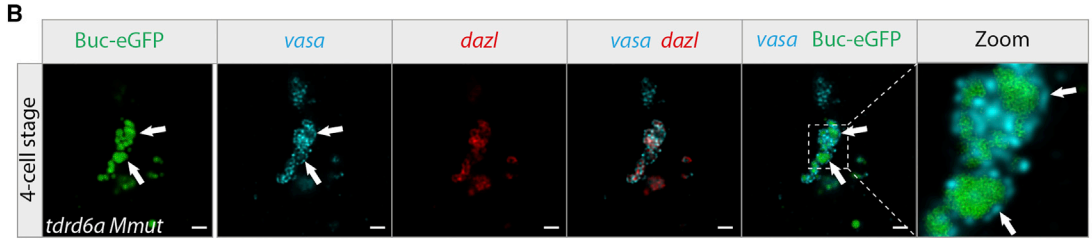

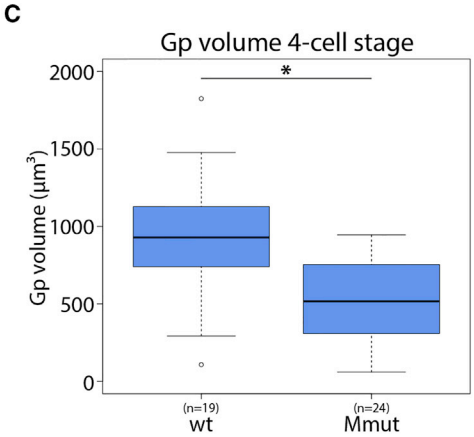

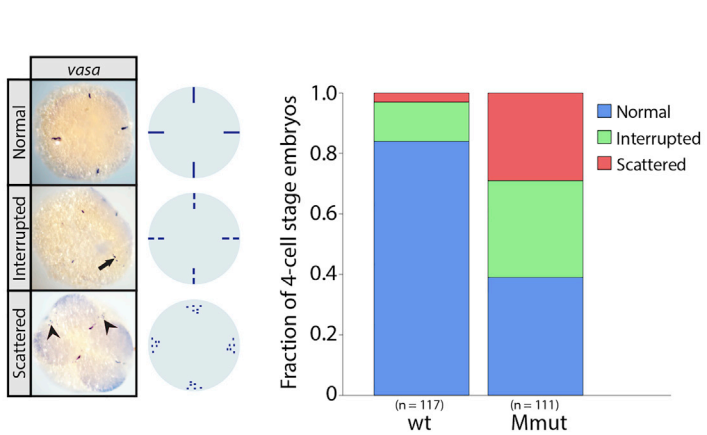

(legend on next page)

We extended these experiments by combining double single-molecule FISH (smFISH) with IHC for Tdrd6a in a Buc-eGFP background (Riemer et al., 2015). In the Bb, Buc-eGFP and Tdrd6a form a continuous structure in which Gp mRNAs are embedded (Figure 3C). SmFISH shows that different Gp transcripts display diverse sub-localization within the Bb. The *dazl* signal is found as a rather compact core in the Bb, whereas *vasa* is found more throughout the entire Bb (Figure 3C). Interestingly, the smFISH signals do not overlap with each other but rather form transcript-specific networks (Figure 3C, line graph). In *tdrd6a* mutant oocytes, the Buc-eGFP signal is more irregular (Figure 3D). Gp-transcripts still localize to the Bb, indicating that Tdrd6a is not essential for these transcripts to accumulate in the Bb (Figure 3D).

Electron microscopy (EM) revealed that the electron-dense structures in the Bb display a heterogeneous, fibrillary appearance (Figures 3E and S4A, yellow overlays). In contrast, Bbs without Tdrd6a have larger and more homogenous electron-dense areas than with Tdrd6a (Figures 3F and S3B, yellow overlays). A more widely conserved function of the Bb is mitochondrial selection, which is therefore highly represented in the Bb (Bilinski et al., 2017). We found that mitochondria still accumulate in the Bb in the absence of Tdrd6a (Figures 3E, 3F, S4A, and S4B, cyan overlays). In conclusion, Tdrd6a is required for the overall organization of the Bb, even though mRNAs and mitochondria are still present.

Tdrd6a Is Required for Merging Particles with Distinct mRNA Content into Mature Gp Structures in the Embryo

In late oogenesis, the Bb disperses into fragments at the vegetal cortex of the oocyte. Upon fertilization, these Buc-containing assemblies accumulate at the cleavage planes to form larger Gp structures (Riemer et al., 2015). Using smFISH and IHC, we found that in 1-cell stage embryos, Buc and Tdrd6a form isolated particles, decorated with discrete mRNA foci at their periphery (Figure 4A, arrowheads). Buc forms the core of the Gp particles, whereas the Tdrd6a signal is predominantly found at the edge (Figure 4A, arrowheads). As in the Bb, transcript signals do not overlap. At the 2-cell stage, the smaller Buc-Tdrd6a units organize themselves along the cleavage planes and start to cluster together (Figure 4A). The Buc signal often bridges individual granules (Figure 4A, arrows). Furthermore, Tdrd6a appears to be localized around the Buc-assemblies, similar to the mRNA (Figure 4A, arrowheads).

The Gp grows further toward the 4-cell stage into a larger structure, in which the Tdrd6a signal surrounds the Buc signal (Figure 4A). We also observe that in these parts of the Gp transcripts have mostly moved inward, forming large intermingled networks (Figure 4A, line graph). Overall, the smFISH signals for different mRNAs are very well mixed within the larger Gp structure, but areas of overall enrichment for one or the other mRNA can still be observed. We note that structures similar to the internal smFISH signal were found using antibody-mediated FISH (Figure S5A), suggesting that the peripheral Tdrd6a signal on Gp does not result from issues related to general antibody penetration into the structure.

In embryos lacking Tdrd6a, mRNAs still associate with Buc particles (Figure 4B), showing that like in the Bb, Tdrd6a is not required for this association. However, without Tdrd6a the Gp structure fails to grow and remains relatively small and highly fragmented (Figures 4C, 4D, and S5B). We do observe some apparent fusion of Buc particles, but typically, also in these cases, mRNA remains at the periphery (Figure 4B, arrows). These observations lead us to propose that Gp forms through the ongoing accumulation of small granules, containing Buc, Tdrd6a, and mRNPs. Tdrd6a contributes to the accumulation of these granules and for the mRNP particles to move into the Buc structure, where they intermingle and form networks with mRNPs of the same kind. We speculate that it is the lack of Gp growth that ultimately results in the above described Gp mRNA defects we see in PGCs lacking Tdrd6a.

Tdrd6a Interacts with Buc via Symmetrically Dimethylated Arginines

The IP-mass spectrometry (MS) experiments on ovary extracts identified Buc as a strong interactor of Tdrd6a (Figure 1D). We also found Buc, as well as the close Tdrd6a paralog Tdrd6c, to be among the strongest interactors of Tdrd6a in freshly laid embryos (Figure 5A). We verified the Buc-Tdrd6a interaction on western blot and show resistance to RNase A treatment (Figure 5B). Tdrds often bind sDMA residues in a binding partner (Siomi et al., 2010). Indeed, analysis of our MS results identified two dimethylated arginine residues within the C terminus of Buc, residing in a tri-RG (RG[X_{0-4}]RG[X_{0-4}]RG) motif (Figure 5C) (Thandapani et al., 2013). In order to test their relevance for interaction with Tdrd6a, we performed pull-down experiments using biotinylated peptides covering these arginines in either an sDMA- or non-methylated state followed by MS. In the pull-down using the methylated Buc-peptide, Tdrd6a was highly enriched (Figure 5D). Interestingly, another Tdrd6 paralog, Tdrd6c, was also among the few enriched proteins. The pull-down with the non-methylated peptide showed enrichment for two members of the serine-arginine protein kinase family, Srpk1a and Srpk1b (Figure 5D), confirming that this pull-down was also successful

Figure 4. Tdrd6a Is Required for Gp Integrity

(A) Confocal images of Buc-eGFP-positive embryos from *tdrd6a*$^{+/-}$ mothers, at 1-, 2-, and 4-cell stages, focusing on Gp as schematically indicated. In zoom of the Gp, IHC for Tdrd6a and double smFISH was performed and displayed as indicated. Arrowheads indicate mRNA and Tdrd6a that is peripherally localized on the Gp granule; arrows indicate Buc-eGFP bridges (zooms 1 and 2 on the right). Asterisks mark mature Gp, containing fused Buc-eGFP and mRNA networks inside the structure. Line graphs display intensity for Buc (green) versus Tdrd6a (red) signals over line a-b and *dazl* (red) versus *vasa* (cyan) intensity over line c-d, with vertical lines indicating fluorescence peaks per smFISH signal (highlighted by colored circle on top).

(B) Confocal images of Buc-eGFP-positive Gp of a 4-cell stage embryo from a *tdrd6a*$^{-/-}$ mother (Mmut). SmFISH was performed and displayed as indicated. Arrows indicate areas where Buc-eGFP has fused, but mRNA remains peripherally localized.

(C) Boxplot representing volumes of the Buc-eGFP signal at the cleavage planes of wt and Mmut 4-cell stage embryos. The largest Gp fragment of each embryo was measured (also see Figure S5B) after 3D reconstruction in Imaris. (* indicates p value < 0.001, Wilcoxon test).

(D) Quantification of Gp phenotypes of 4-cell stage embryos using an ISH against *vasa*. Scale bars, 10 μm (overview A), 2 μm (zoom) (A), and 2 μm (B).

See also Figure S5.

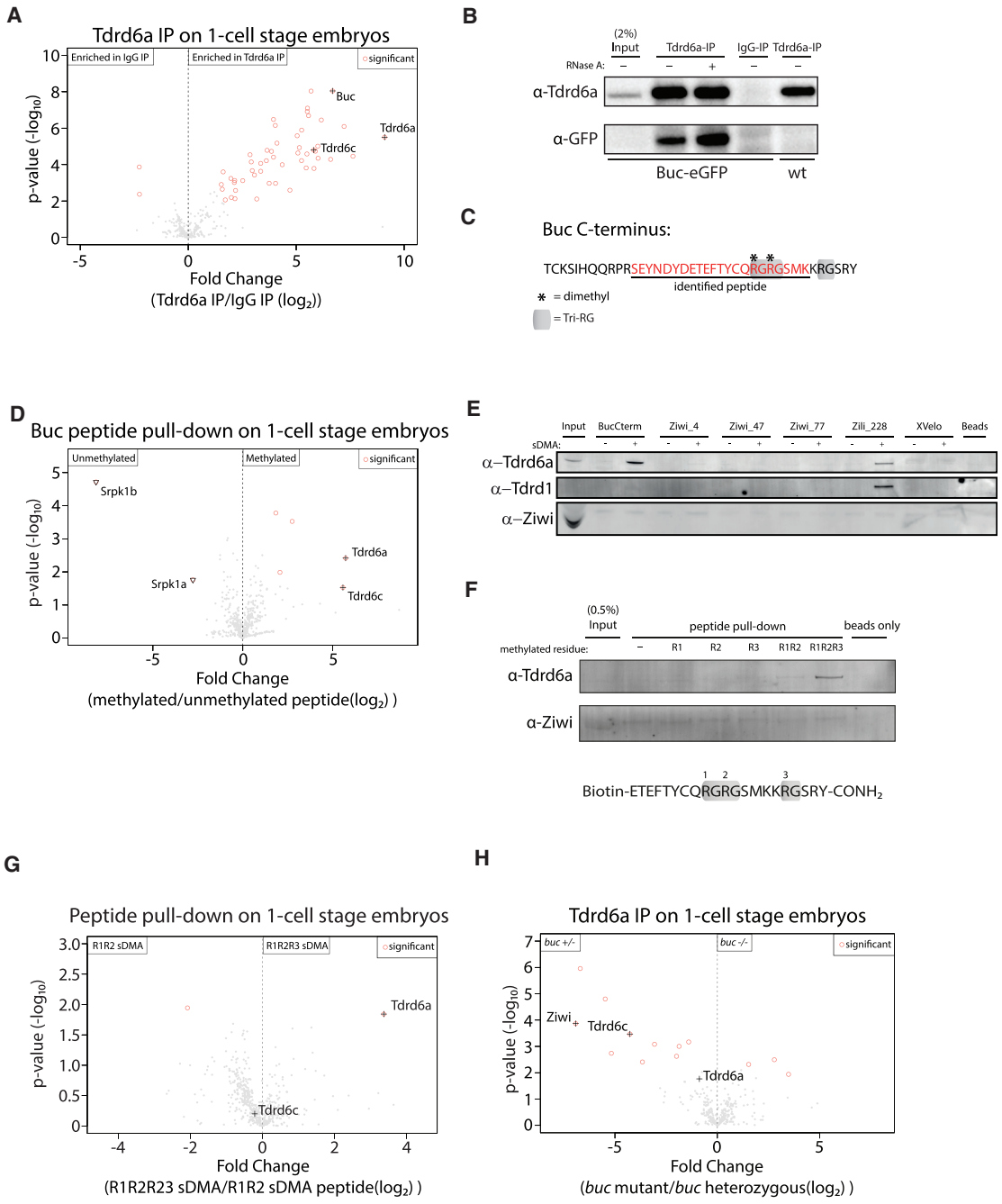

Figure 5. Tdrd6a and Buc Interact via sDMAs in the C Terminus of Buc

(A) Volcano plot of Tdrd6a IP compared to IgG IP on embryo extracts, followed by MS.

(B) Confirmation of Tdrd6a co-IP with Buc using the Buc-eGFP transgenic line.

(C) C terminus of Buc with the identified dimethylated peptide underlined. Asterisk indicates residues that were found to be dimethylated by MS. Three RG sites together form a tri-RG motif, indicated in gray.

(D) Volcano plot of peptide pull-down on embryo extracts followed by MS. On the "Methylated" peptide, all 3 RG motifs were symmetrically dimethylated.

(E) Peptide pull-down followed by western blot for multiple methylated (sDMA) and non-methylated peptides derived from proteins known to contain sDMA modifications and the Buc homolog XVelo on ovary extracts. Listed are all peptides used.

(F) Peptide pull-down of Buc C terminus peptides with different methylation states on embryo extracts.

(G) MS of pull-downs of double and triple sDMA modified peptides.

(H) MS of Tdrd6a IP in the *buc*$^{+/-}$ compared to *buc*$^{-/-}$ background. Tdrd6c and Ziwi are specifically enriched in the buc$^{+/-}$ background, indicating that they require the presence of Buc to associate with Tdrd6a.

A

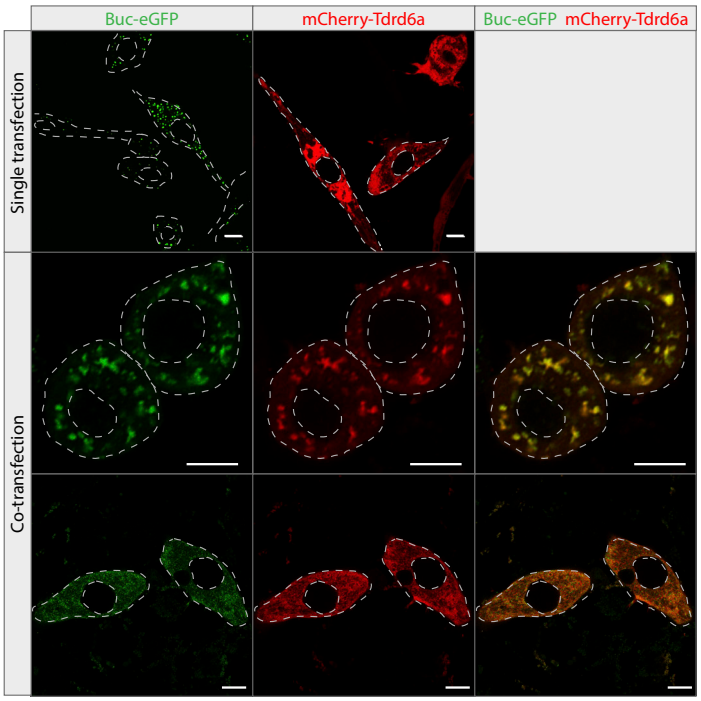

B

Day 1 Buc	Day 2 Tdrd6a	Day 3 Imaging	+ Buc	- Buc
Tdrd6a aggregated			23	0
Tdrd6a dissolved			0	32

C

Day 1 Tdrd6a	Day 2 Buc	Day 3 Imaging	+ Tdrd6a	- Tdrd6a
Buc small granules			0	27
Buc dissolved			28	0
Buc big granules*			18	0

* Faint Tdrd6a signal only

D

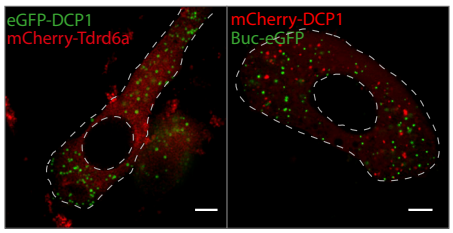

E

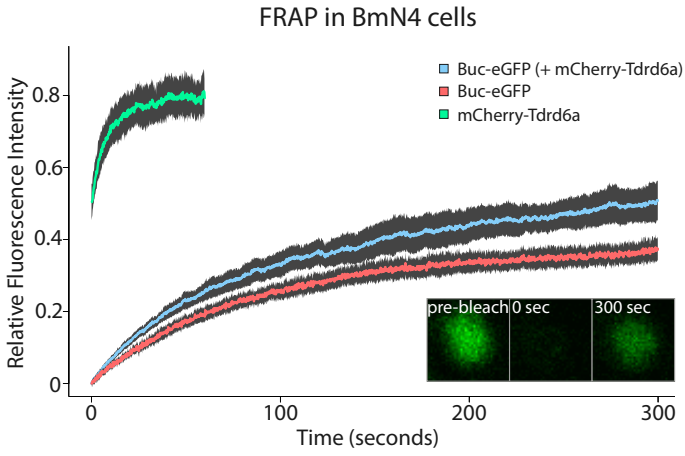

F

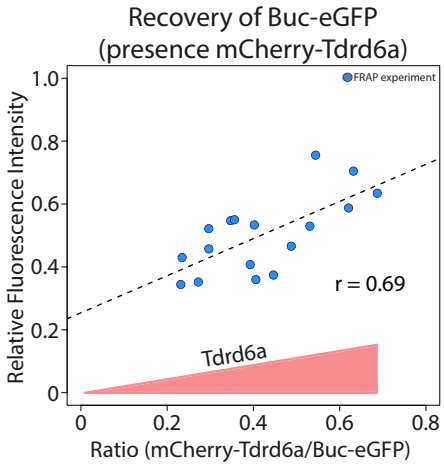

G

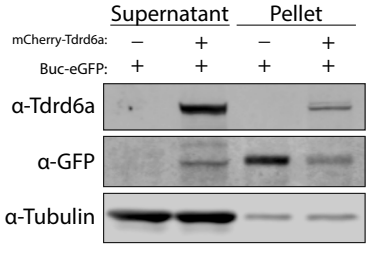

H

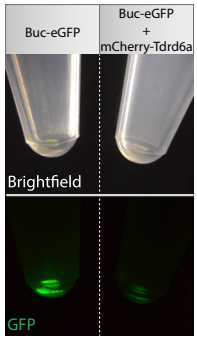

(legend on next page)

and revealing potential additional post-translational regulation of Buc besides sDMAs. To test the specificity of the Buc peptide for Tdrd6a, we repeated the pull-down using peptides derived from Ziwi, Zili, and the analogous C-terminal region of the *Xenopus* Buc homolog XVelo. Clear enrichment of Tdrd6a was found using the methylated Buc peptide, but not using the non-methylated Buc peptide (Figure 5E). We do see some affinity of Tdrd6a for the methylated Zili peptide previously shown to interact with Tdrd1 (Huang et al., 2011). Since Zili is not maternally provided, this affinity could be biologically relevant in ovarian nuage where Zili interacts with Tdrd6a (Figure S2A). Tdrd1 displayed affinity only for the methylated Zili228 peptide, as shown before (Huang et al., 2011), and did not interact with the sDMAs residing in the Buc C terminus (Figure 5E). Moreover, we found that all three sDMAs on the Buc peptide are required for Tdrd6a interaction (Figure 5F). Interestingly, MS analysis demonstrated that Tdrd6c does bind to both the di- and tri-methylated Buc peptides (Figure 5G). Lastly, Tdrd6a IP/MS from *buc*$^{+/-}$ and *buc*$^{-/-}$ embryos showed that without Buc, Tdrd6c (and also Ziwi) is lost from Tdrd6a IPs (Figure 5H). We conclude that both Tdrd6a and Tdrd6c specifically interact with sDMA-modified Buc and that they may be responsible for recruitment of different protein complexes to Gp.

Tdrd6a Affects the Aggregation Behavior of Buc

It has been shown previously that XVelo is a protein with an N-terminal PrD that has a tendency to self-aggregate. We showed that Buc aggregation, illustrated by detailed Bb and Gp imaging, is highly regulated *in vivo* and affected by Tdrd6a. We reasoned that Tdrd6a might be involved in spatiotemporal regulation of Buc aggregation. We first tested this in a heterologous cell culture system, using silkworm-derived BmN4 cells. These are of ovarian origin and cultured at 27°C, the same temperature at which zebrafish are kept, thereby mimicking natural conditions for Tdrd6a and Buc. IP-MS experiments on transfected Buc-eGFP revealed the same arginine methylation on Buc as observed in zebrafish (data not shown). Expression of Buc in BmN4 cells results in abundant, cytoplasmic, small granules (Figure 6A). In contrast, Tdrd6a displays a ubiquitous cytoplasmic signal (Figure 6A). Upon co-transfection, we observe two possible outcomes: the presence of both Tdrd6a and Buc either results in co-localization in enlarged, cytoplasmic aggregates with a broad variety in size (Figures 6A, middle row, and S6A) or in diffuse cytoplasmic localization of both proteins (Figure 6A, bottom row). We then performed consecutive transfection rather than co-transfection and quantified protein behavior. If we first transfect Buc, followed by Tdrd6a the next day, we always observed enlarged granules that are positive for both Buc and Tdrd6a (Figure 6B). When the order of transfection is reversed, Buc mostly localizes throughout the cytoplasm (Figure 6C). Only when the Tdrd6a signal is low, Buc seems to be able to form enlarged granules. This mutual effect between Buc and Tdrd6a is specific, since co-transfection of Buc and Tdrd6a with Dcp1, a P-body marker, leaves both proteins unaffected (Figure 6D). These results demonstrate that Tdrd6a can either stimulate the accumulation of Buc into larger granules or prevent its aggregation altogether.

We investigated the properties of these granules in more detail using fluorescence recovery after photobleaching (FRAP). Tdrd6a recovers rapidly upon bleaching of Buc-Tdrd6a double-positive granules, reflecting a high mobility in and out of the granule (Figure 6E, n = 17). Buc alone only recovers up to ~35% (n = 17) of the initial fluorescence intensity. Interestingly, Buc recovery increases to ~55% (n = 17) in the presence of Tdrd6a (Figure 6E). Quantification of the FRAP experiments shows that this increase in Buc recovery in the presence of Tdrd6a is significant (Figure S6B). However, we did observe a rather broad distribution in recovery in Tdrd6a-Buc double-positive granules (Figure S6B). We hypothesized that this variation in Buc recovery could be due to differences in relative Buc and Tdrd6a concentrations in the granules that were studied. Hence, we normalized the protein amounts in the FRAP experiments by calibrating relative fluorescence using an mCherry-eGFP construct (Figure S6C). This revealed that the more Tdrd6a is present in a granule, the better Buc can recover (Figure 6F). Furthermore, without Tdrd6a Buc-eGFP cannot be detected in the soluble fraction of BmN4 lysates and is predominantly found in the pellet (Figures 6G and 6H). In contrast, in the presence of Tdrd6a, significant amounts of Buc-eGFP were soluble (Figure 6G). We conclude that Tdrd6a positively stimulates Buc mobility and solubility and that this can contribute to growth of Buc granules.

The tri-RG Motif of Buc Is Required for Bb Formation

We then aimed to test the *in vivo* relevance of the FRAP results and the Tdrd6a-Buc interaction data we describe in Figure 5. First, we performed FRAP on the Bb of Buc-eGFP-positive oocytes in *tdrd6a*$^{+/-}$ and $^{-/-}$ backgrounds. These studies showed a remarkable decrease of mobility of Buc within the Bb in the absence of Tdrd6a (Figure 7A). Second, we created a line that expresses a modified version of Buc-eGFP in which we replaced the arginine residues in the C-terminal tri-RG motif

Figure 6. Tdrd6a Stimulates Buc Mobility in BmN4 Cells

(A) Localization of Buc-eGFP and mCherry-Tdrd6a in BmN4 cells in a single transfection (upper panel) and when they are co-transfected (middle and bottom). Co-transfected BmN4 cells displaying enlarged Buc-eGFP granules to which mCherry-Tdrd6a co-localizes (middle) or dissolved Buc-eGFP (bottom). Scale bars, 10 μm.

(B) Quantification of localization of Tdrd6a transfected 1 day after Buc.

(C) Quantification of localization of Buc transfected 1 day after Tdrd6a.

(D) Co-transfection of Dcp1-mCherry with Buc-eGFP (left) or Dcp1-eGFP with mCherry-Tdrd6a (right). Scale bars, 5 μm.

(E) FRAP recovery curves of mCherry-Tdrd6a and Buc-eGFP (with or without the presence of mCherry-Tdrd6a as indicated). Fluorescence intensity is the calculated fraction of the pre-bleach intensity and is plotted with the 95% confidence interval.

(F) FRAP recovery of Buc-eGFP plotted against increasing relative amounts of mCherry-Tdrd6a present in the bleached granule.

(G) Western blot for GFP and Tdrd6a on transfected BmN4 cell lysates and corresponding pellets.

(H) Pellets of lysates of Buc-EGFP-expressing BmN4 cells in the presence or absence of Tdrd6a as indicated.

See also Figure S6.

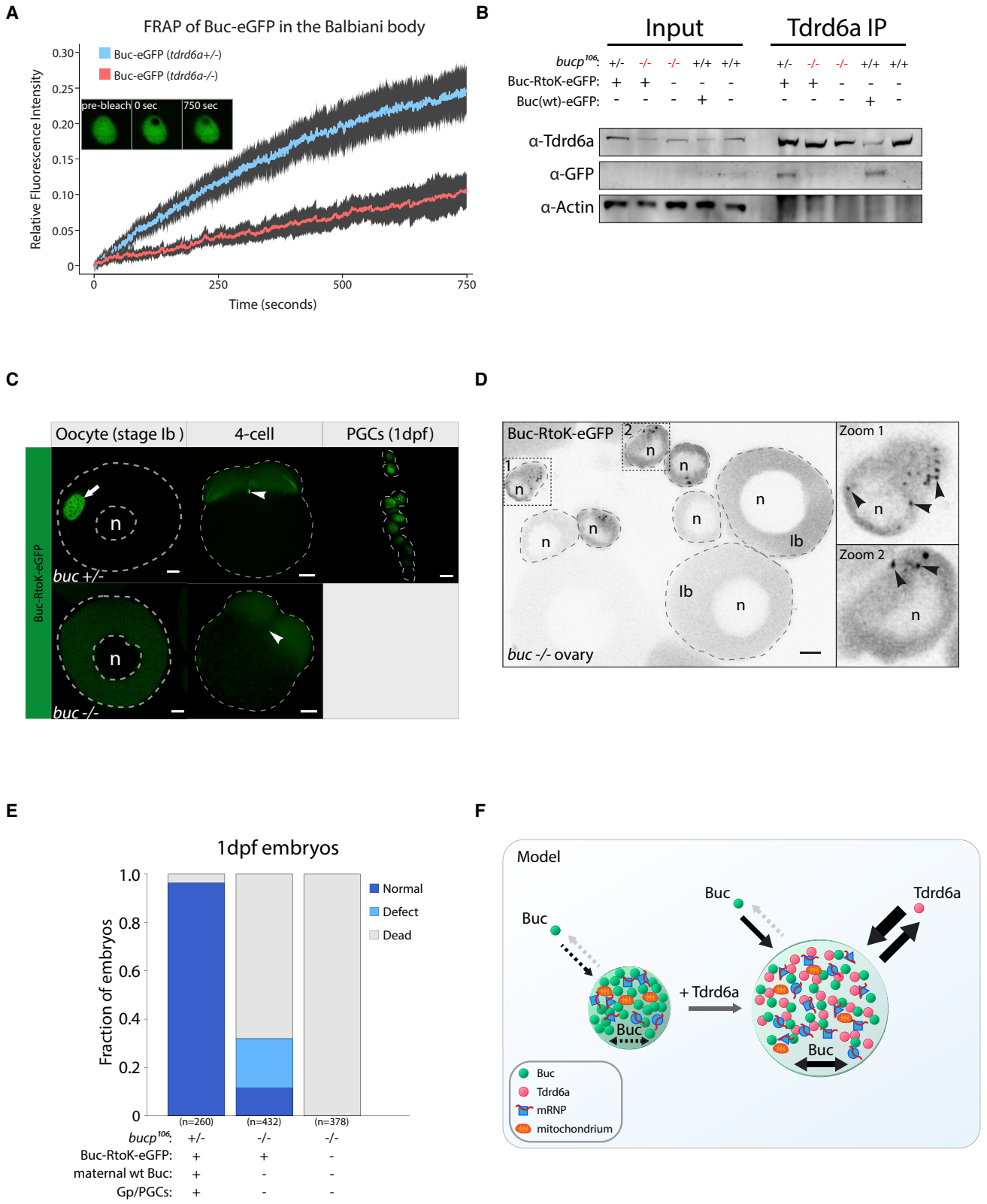

Figure 7. Tdrd6a Stimulates Buc-eGFP Mobility *In Vivo*

(A) FRAP recovery curves of Buc-eGFP in *tdrd6a* heterozygous or mutant Balbiani bodies. Fluorescence intensity is the calculated fraction of the pre-bleach intensity and plotted with a 95% confidence interval.

(legend continued on next page)

by lysines (Buc-RtoK). In the presence of wt Buc, Buc-RtoK can interact with Tdrd6a (Figure 7B), can be incorporated into the Bb and Gp, and is found in PGCs 1 day post fertilization (dpf) (Figure 7C). In contrast, in the absence of wt Buc, Buc-RtoK does not interact with Tdrd6a (Figure 7B) and fails to form a Bb in stage-Ib oocytes (Figures 7C and S7A). Tdrd6a still localizes to nuage in these oocytes (Figure S7A). Furthermore, in the absence of wt Buc, Buc-RtoK embryos neither have Gp at the 4-cell stage cleavage planes nor form PGCs (Figure 7C). Buc-RtoK alone does form small granules in early stage-I oocytes (ø < ~30 μm), but these are detached from the nucleus and never progress to form a Bb (Figure 7D, arrowheads). Despite the absence of a Bb, Buc-RtoK embryos are polarized and are partly viable (Figures 7E and S7B), indicating that Buc-RtoK can partly rescue the *buc* phenotype and that polarization is Bb-independent. However, most embryos do show severe defects in cell division and/or subsequent development (Figures 7E and S7B).

In conclusion, our data show that Tdrd6a and its interaction with arginine-methylated Buc affect the aggregation behavior of Buc-containing structures by stimulating their growth, heterogeneity, and mobility (Figure 7F), both in cell culture as well as *in vivo*, and that this is directly relevant for germ cell formation and embryonic development.

DISCUSSION

Proteins such as Tdrd6a, with multiple Tudor domains in tandem, are well known to act in germ cells, in particular in smRNA pathways and their organization in peri-nuclear granules. Their precise molecular functions, however, are far from resolved. Other highly abundant components of germ cells are proteins with low-complexity regions and/or PrDs, such as Buc. Other examples are MUT-16 and MEG proteins in *C. elegans*, and Xvelo in *Xenopus*, which nucleate a variety of subcellular aggregates (Boke et al., 2016; Phillips et al., 2012; Wang et al., 2014). However, insights into how their aggregation behavior is regulated remain scarce. We demonstrate that Tdrd6a regulates the aggregation of Buc. More specifically, it promotes solubility and mobility of Buc, and thereby growth of Buc aggregates into larger structures containing well-determined amounts of germ cell-specifying mRNPs and other Gp components. Various aspects related to our findings will be further discussed here.

Tdrd6a Does Not Affect piRNA Generation

Even though the Piwi proteins appear to interact with Tdrd6a in ovary extracts, lack of Tdrd6a does not have an effect on piRNA accumulation. Given the intimate connection between piRNA biogenesis and function, a mechanistic role for Tdrd6a in the piRNA pathway does not seem likely. Our results suggest, however, that Tdrd6c, instead of Tdrd6a, is the more relevant interaction partner for the piRNA pathway. Analysis of *tdrd6c* mutants will be required to clarify this.

Molecular Basis behind the PGC Phenotype of tdrd6a Mutants

We observed that Gp arises from the continuous merging of smaller Buc-Tdrd6a granules in embryos. In these granules, Buc is found at the core, while we detected Tdrd6a mainly at the periphery. We note, however, that at present, we cannot be certain that this apparent substructure is real, or whether it represents an experimental artefact due to very high local Tdrd6a concentrations surrounding the Gp structure.

The individual Buc-Tdrd6a granules in 1–2 cell embryos display discrete mRNA foci at their circumference. Interestingly, these foci move more internally and start to form networks when larger assemblies arise. Homotypic assemblies of mRNPs have been described recently in *Drosophila*, where it has been demonstrated that Gp mRNAs initially form homogenous mRNP granules, followed by fusion into heterogeneous mRNP aggregates, in which the quantities of Gp mRNAs positively correlate (Little et al., 2015; Trcek et al., 2015). In zebrafish, we could infer that mRNA quantities in mature Gp positively correlate as well and that Tdrd6a is required for this.

Why does this correlation between Gp mRNAs depend on Tdrd6a? In absence of Tdrd6a, mostly small incomplete Gp-like structures are found. Given that each Tdrd6a-Buc granule at the 1–2 cell stage only carries a limited number of individual mRNPs, sufficiently large numbers of Buc-Tdrd6a granules need to accumulate to attain the ratios as found on all granules combined. Without Tdrd6a, these numbers may not be reached. Since single Gp mRNAs can have a strong impact on PGC formation, such unstable ratios may directly relate to the observed PGC specification and/or maintenance defects.

mRNP Recruitment and Organization in Gp

Single Buc-containing particles contain individual foci of various Gp transcripts at their periphery. We show that this does not require Tdrd6a. How then are these transcripts recruited? Intrinsic properties, such as primary sequence or secondary structure of the mRNPs, may play a role (Knaut et al., 2002; Köprunner et al., 2001; Trcek et al., 2015). Furthermore, the fact that we identify the cytoplasmic EJC complex and the CPEB complex in our Tdrd6a interactome may reveal an additional aspect: mRNPs that have not undergone translation could be prone to be incorporated into Gp-related structures. Indeed, these complexes have been demonstrated to play a role in

(B) Tdrd6a IPs probed for the indicated proteins by western blot. Buc^{p106} = *buc* loss-of-function allele. Note that Buc-eGFP is typically very hard to detect in total lysates.

(C) Localization of Buc-RtoK-eGFP in the $buc^{+/-}$ and $buc^{-/-}$ background. Arrow indicates Bb, arrowheads indicate Gp ($buc^{+/-}$) or where Gp should be ($buc^{-/-}$). Scale bars for oocyte and 1dpf, 10 μm. Scale bar for 4-cell, 100 μm. n = nucleus.

(D) Overview of $buc^{-/-}$ ovary (whole mount) positive for Buc-RtoK-eGFP. Zooms 1 and 2 are examples of stage-I oocytes ø < ~30 μm, containing small Buc-RtoK-positive granules (arrowheads). These granules are never detected in stage-Ib oocytes, where Buc-RtoK is diffusely cytoplasmic. Scale bar, 10 μm, n = nucleus.

(E) Quantification of progeny viability at 1 dpf spawned by mothers with background as indicated, crossed with wt males.

(F) Model of Buc-containing granules, with or without Tdrd6a. Arrows indicate movement in and out of the structure or mobility within the structure itself.

See also Figure S7.

translational control and/or Gp transcript localization in *Drosophila* and *Xenopus* (Hachet and Ephrussi, 2004; Minshall et al., 2007; Nelson et al., 2004).

In more enlarged Gp structures, we observe bigger transcript networks, each consisting of single types of mRNA that spread throughout the Gp. Possibly, intrinsic properties of mRNPs trigger such network formation when local concentrations are sufficiently high. Indeed, the intrinsic tendency of transcripts of the same kind to cluster is a phenomenon that has been suggested previously in *Drosophila* (Little et al., 2015; Trcek et al., 2015). These larger homotypic structures may subsequently be further stabilized by their continued interaction with the growing Buc-containing structure, in which they intermingle with other homotypic networks. Our data show that Tdrd6a is required for this higher level organization of Gp mRNPs. Whether this results from its effect on Buc or on mRNPs directly cannot be distinguished at present.

How Does Tdrd6a Regulate Buc Aggregation?

We describe potentially contradicting effects of Tdrd6a on Buc behavior: on the one hand, Tdrd6a promotes Buc solubility and/or mobility, and, on the other hand, Tdrd6a drives the formation of larger Buc aggregates. Based on our cell culture experiments, we speculate that the effect of Tdrd6a on Buc may critically depend on relative and absolute concentrations of both proteins. Possibly, the multi-tudor domain organization of Tdrd6a/c allows it to increase local Buc concentrations, and hence Buc aggregation behavior. But at the same time, the high mobility of Tdrd6a, and possibly also Tdrd6c, may drive constant remodeling of Buc aggregates and prevent the formation of too rigid or too many condensed Buc aggregates and allow fusion and/or growth of Buc aggregates. To address these possibilities, *in vitro* systems will need to be established, such that protein-protein interactions and aggregation behavior can be studied in much greater detail.

Regardless of the exact mechanisms, our work reveals that post-translational modifications (PTMs) can play an important role in how aggregations are regulated: loss of Buc arginine methylation, and hence Tdrd6a interaction, severely affects Buc behavior *in vivo*. In fact, the RtoK mutations in Buc result in a much more severe phenotype than that observed in *tdrd6a* mutants. We consider it likely that this is caused by additional loss of Tdrd6c interactions with Buc. Possibly, additional PTMs and their dynamics are involved in the complex aggregation behavior that Buc displays *in vivo* but also in other scenarios. For instance, during early embryogenesis in *C. elegans*, phosphorylation and dephosphorylation of MEG-1/3 (maternal effect germ-cell defective 1 and 3) control P granule disassembly and assembly, respectively (Wang et al., 2014). Since kinases were identified in the non-modified Buc peptide pull-down, it is tempting to speculate that besides arginine dimethylation, phosphorylation may also regulate Buc aggregation dynamics.

The Bb Is Not Required for Generating Oocyte Polarity

We found that Buc-RtoK can rescue the oocyte polarization defect of *buc* mutants, even though a Bb never forms. This shows that the Bb as such is not essential for oocyte polarity establishment and that Buc may have a Bb-independent role that helps to maintain or establish polarity. Nevertheless, we did observe that Buc-RtoK could not fully rescue the loss of endogenous Buc because many embryos did not develop properly. This is unlikely to be due to tag interference since wt transgenic Buc that also carries a GFP tag at its C terminus can fully rescue (Riemer et al., 2015). Therefore, Buc and/or the Bb may play important roles downstream of polarity establishment in the oocyte as well.

Buc-Tdrd6a Interaction as a Model for Regulated Protein Aggregation

Phase separation of proteins with IDRs has been recognized as a research field of major importance. It represents a pivotal type of compartmentalization, which mediates diverse cellular processes. There appears to be a wide range of aggregation states, spanning from liquid-like droplets to almost solid aggregations (Brangwynne et al., 2011; Patel et al., 2015; Shin and Brangwynne, 2017). It has been proposed that pathogenic protein aggregates, such as those found in Alzheimer disease or amyotrophic lateral sclerosis (ALS), represent a detrimental state of normally occurring protein aggregation. Hence, knowledge about how aggregation states can be regulated *in vivo* will be directly relevant to the understanding of these types of disease. Since Buc aggregation is very dynamic during zebrafish oogenesis and embryogenesis, it represents a powerful model to study the spatiotemporal regulation of protein aggregation, both by trans-acting factors as well as PTMs.

Analogous to previous studies, Buc typically behaves like a "scaffold," recovering slowly and only partially. Tdrd6a recovery is typical for a granule "client," displaying rapid, near complete recovery, indicating high mobility in and out of the Buc-aggregate (Woodruff et al., 2017). This may mean that in other scenarios in which Tdrd6a-like proteins have been described to affect aggregations, such as for example, the chromatoid body in mammalian spermatocytes or peri-nuclear nuage, scaffold proteins such as Buc are still to be discovered. Alternatively, well-known proteins may in fact act as such scaffolds. For instance, Piwi proteins typically have rather long and seemingly unstructured N-terminal tails, and also other well-studied proteins, like Vasa, contain disordered regions and can phase separate *in vitro* (Nott et al., 2015). Indeed, these proteins are rich in RG motifs that could be sites of aggregation modulation by Tdrd proteins.

STAR★METHODS

Detailed methods are provided in the online version of this paper and include the following:

- KEY RESOURCES TABLE
- CONTACT FOR REAGENT AND RESOURCE SHARING
- EXPERIMENTAL MODEL AND SUBJECT DETAILS
  - Zebrafish Lines
  - Cell Culture
- METHOD DETAILS
  - Genotyping
  - Tdrd6a Antibody
  - Whole Mount Colorimetric In Situ Hybridization Embryos
  - Whole Mount Fluorescent In Situ Hybridization

- Whole Mount Double smFISH and IHC
- Peptide Pull-Down
- FRAP
- Immunohistochemistry
- Confocal Imaging
- Immunoprecipitation
- Western Blot
- Library Construction and High-Throughput Sequencing
- Bioinformatic Analysis
- LC-MS/MS
- Data Analysis
- Fluorescence-Activated Cell Sorting (FACS)
- CEL-Seq Library Preparation
- Quantification of Transcript Abundance
- RaceID2
- Detection of Differentially Expressed Genes in scRNA-Seq Data
- Background Correlation Model and Random Cell Generation
- qPCR
- RIP-Seq
- Morpholino Knockdown and PGC Quantification
- Electron Microscopy
- BmN4 Cell Transfection
- Cloning

- QUANTIFICATION AND STATISTICAL ANALYSIS
- DATA AND SOFTWARE AVAILABILITY

SUPPLEMENTAL INFORMATION

Supplemental Information includes seven figures and can be found with this article online at https://doi.org/10.1016/j.devcel.2018.07.009.

ACKNOWLEDGMENTS

We thank the members of our laboratory for fruitful discussions. Yasmin El Sherif is thanked for extensive experimental support. We thank the Cuppen group (Hubrecht) for identifying the *tdrd6a*^{Q158X} allele. We would like to thank Jeroen Krijsgveld and the proteomics core facility at EMBL for performing initial proteomics analysis and Eugene Berezikov (Hubrecht/ERIBA) for initial bioinformatics support. We thank the following IMB Core Facilities for their contributions and valuable services: genomics, microscopy, bioinformatics, flow cytometry, and the media lab. In particular, we thank Mária Hanulová for support in FRAP experiments. We thank Edward Lemke for critical reading of the manuscript. This work was supported by the Rhineland Palatinate Forschungsschwerpunkt GeneRED, a Marie Curie fellowship 623119 (L.J.T.K.), the ERC (ERC-StG202819, R.F.K., and ERC-AdG294325-GeneNoiseControl, A.v.O.), and Vici award 724.011.001 (R.F.K.) from the Nederlandse Organisatie voor Wetenschappelijk Onderzoek (NWO).

AUTHOR CONTRIBUTIONS

E.F.R., L.J.T.K., and R.F.K. conceived the study and designed experiments. L.J.T.K. performed scRNA-seq experiments and data analysis, RIP-seq analysis, and some of the IP experiments. E.F.R. performed most other experiments. S. Redl performed electron microscopy experiments, with assistance of W.S. A.W.B. performed BmN4 cell culture experiments. A.M.d.J.D. performed smRNA-seq analysis. H.Y.H. performed initial analyses of the *tdrd6a* mutant and Tdrd6a localization. S.Riemer and R.D. provided the wt Buc-eGFP construct and transgenic line. K.W. performed scRNA-seq experiments, and D.G. and A.v.O devised scRNA-seq data analyses. C.T.H. optimized RIP-seq protocols, and F.B. performed MS analysis. R.F.K. supervised the project. L.J.T.K., E.F.R., and R.F.K. wrote the paper with input from all authors.

DECLARATION OF INTERESTS

The authors declare no competing interests.

Received: December 5, 2017
Revised: April 23, 2018
Accepted: July 11, 2018
Published: August 6, 2018

REFERENCES

Akpınar, M., Lesche, M., Fanourgakis, G., Fu, J., Anastassiadis, K., Dahl, A., and Jessberger, R. (2017). TDRD6 mediates early steps of spliceosome maturation in primary spermatocytes. PLoS Genet. *13*, e1006660.

Anders, S., and Huber, W. (2010). Differential expression analysis for sequence count data. Genome Biol. *11*, R106.

Barckmann, B., Pierson, S., Dufourt, J., Papin, C., Armenise, C., Port, F., Grentzinger, T., Chambeyron, S., Baronian, G., Desvignes, J.P., et al. (2015). Aubergine iCLIP reveals piRNA-dependent decay of mRNAs involved in germ cell development in the early embryo. Cell Rep. *12*, 1205–1216.

Bilinski, S.M., Kloc, M., and Tworzydlo, W. (2017). Selection of mitochondria in female germline cells: is Balbiani body implicated in this process? J. Assist. Reprod. Genet. *34*, 1405–1412.

Blaser, H., Eisenbeiss, S., Neumann, M., Reichman-Fried, M., Thisse, B., Thisse, C., and Raz, E. (2005). Transition from non-motile behaviour to directed migration during early PGC development in zebrafish. J. Cell Sci. *118*, 4027–4038.

Boke, E., Ruer, M., Wühr, M., Coughlin, M., Lemaitre, R., Gygi, S.P., Alberti, S., Drechsel, D., Hyman, A.A., and Mitchison, T.J. (2016). Amyloid-like self-assembly of a cellular compartment. Cell *166*, 637–650.

Bontems, F., Stein, A., Marlow, F., Lyautey, J., Gupta, T., Mullins, M.C., and Dosch, R. (2009). Bucky ball organizes germ plasm assembly in zebrafish. Curr. Biol. *19*, 414–422.

Brangwynne, C.P., Eckmann, C.R., Courson, D.S., Rybarska, A., Hoege, C., Gharakhani, J., Julicher, F., and Hyman, A.A. (2009). Germline P granules are liquid droplets that localize by controlled dissolution/condensation. Science *324*, 1729–1732.

Brangwynne, C.P., Mitchison, T.J., and Hyman, A.A. (2011). Active liquid-like behavior of nucleoli determines their size and shape in Xenopus laevis oocytes. Proc. Natl. Acad. Sci. USA *108*, 4334–4339.

Brennecke, J., Aravin, A.A., Stark, A., Dus, M., Kellis, M., Sachidanandam, R., and Hannon, G.J. (2007). Discrete small RNA-generating loci as master regulators of transposon activity in Drosophila. Cell *128*, 1089–1103.

Brennecke, J., Malone, C.D., Aravin, A.A., Sachidanandam, R., Stark, A., and Hannon, G.J. (2008). An epigenetic role for maternally inherited piRNAs in transposon silencing. Science *322*, 1387–1392.

Cox, J., and Mann, M. (2008). MaxQuant enables high peptide identification rates, individualized p.p.b.-range mass accuracies and proteome-wide protein quantification. Nat. Biotechnol. *26*, 1367–1372.

Grün, D., Kester, L., and van Oudenaarden, A. (2014). Validation of noise models for single-cell transcriptomics. Nat. Methods *11*, 637–640.

Grün, D., Lyubimova, A., Kester, L., Wiebrands, K., Basak, O., Sasaki, N., Clevers, H., and van Oudenaarden, A. (2015). Single-cell messenger RNA sequencing reveals rare intestinal cell types. Nature *525*, 251–255.

Grün, D., Muraro, M.J., Boisset, J.C., Wiebrands, K., Lyubimova, A., Dharmadhikari, G., van den Born, M., van Es, J., Jansen, E., Clevers, H., et al. (2016). De novo prediction of stem cell identity using single-cell transcriptome data. Cell Stem Cell *19*, 266–277.

Hachet, O., and Ephrussi, A. (2004). Splicing of oskar RNA in the nucleus is coupled to its cytoplasmic localization. Nature *428*, 959–963.

Harris, A.N., and Macdonald, P.M. (2001). Aubergine encodes a Drosophila polar granule component required for pole cell formation and related to eIF2C. Development *128*, 2823–2832.

Hashimoto, Y., Maegawa, S., Nagai, T., Yamaha, E., Suzuki, H., Yasuda, K., and Inoue, K. (2004). Localized maternal factors are required for zebrafish germ cell formation. Dev. Biol. *268*, 152–161.

Hashimshony, T., Wagner, F., Sher, N., and Yanai, I. (2012). CEL-seq: single-cell RNA-seq by multiplexed linear amplification. Cell Rep. *2*, 666–673.

Houwing, S. (2009). Piwi-piRNA complexes in the zebrafish germline (Utrecht University Repository), Dissertation.

Houwing, S., Kamminga, L.M., Berezikov, E., Cronembold, D., Girard, A., van den Elst, H., Filippov, D.V., Blaser, H., Raz, E., Moens, C.B., et al. (2007). A role for Piwi and piRNAs in germ cell maintenance and transposon silencing in zebrafish. Cell *129*, 69–82.

Huang, H.Y., Houwing, S., Kaaij, L.J.T., Meppelink, A., Redl, S., Gauci, S., Vos, H., Draper, B.W., Moens, C.B., Burgering, B.M., et al. (2011). Tdrd1 acts as a molecular scaffold for Piwi proteins and piRNA targets in zebrafish. EMBO J. *30*, 3298–3308.

Ikenishi, K. (1998). Germ plasm in Caenorhabditis elegans, Drosophila and Xenopus. Dev. Growth Differ. *40*, 1–10.

Junker, J.P., Noël, E.S., Guryev, V., Peterson, K.A., Shah, G., Huisken, J., McMahon, A.P., Berezikov, E., Bakkers, J., and Van Oudenaarden, A. (2014). Genome-wide RNA tomography in the zebrafish embryo. Cell *159*, 662–675.

Karnovsky, M.J. (1965). A formaldehyde-glutaraldehyde fixative of high osmolality for use in electron microscopy. J. Cell Biol. *27*, 137A.

Kato, M., Han, T.W., Xie, S., Shi, K., Du, X., Wu, L.C., Mirzaei, H., Goldsmith, E.J., Longgood, J., Pei, J., et al. (2012). Cell-free formation of RNA granules: low complexity sequence domains form dynamic fibers within hydrogels. Cell *149*, 753–767.

Kirino, Y., Vourekas, A., Sayed, N., de Lima Alves, F., Thomson, T., Lasko, P., Rappsilber, J., Jongens, T.A., and Mourelatos, Z. (2010). Arginine methylation of aubergine mediates Tudor binding and germ plasm localization. RNA *16*, 70–78.

Kloc, M., Bilinski, S., and Etkin, L.D. (2004). The Balbiani body and germ cell determinants: 150 years later. Curr. Top. Dev. Biol. *59*, 1–36.

Knaut, H., Steinbeisser, H., Schwarz, H., and Nüsslein-Volhard, C. (2002). An evolutionary conserved region in the vasa 3'UTR targets RNA translation to the germ cells in the zebrafish. Curr. Biol. *12*, 454–466.

Köprunner, M., Thisse, C., Thisse, B., and Raz, E. (2001). A zebrafish nanos-related gene is essential for the development of primordial germ cells. Genes Dev. *15*, 2877–2885.

Kroschwald, S., Maharana, S., Mateju, D., Malinovska, L., Nüske, E., Poser, I., Richter, D., and Alberti, S. (2015). Promiscuous interactions and protein disaggregases determine the material state of stress-inducible RNP granules. Elife *4*, e06807.

Krøvel, A.V., and Olsen, L.C. (2004). Sexual dimorphic expression pattern of a splice variant of zebrafish vasa during gonadal development. Dev. Biol. *271*, 190–197.

Krøvel, A.V., and Olsen, L.C. (2002). Expression of a vas::EGFP transgene in primordial germ cells of the zebrafish. Mech. Dev. *116*, 141–150.

Kwan, K.M., Fujimoto, E., Grabher, C., Mangum, B.D., Hardy, M.E., Campbell, D.S., Parant, J.M., Yost, H.J., Kanki, J.P., Chien, C.B., et al. (2007). The Tol2kit: a multisite gateway-based construction kit for Tol2 transposon transgenesis constructs. Dev. Dyn. *236*, 3088–3099.

Leu, D.H., and Draper, B.W. (2010). The ziwi promoter drives germline-specific gene expression in zebrafish. Dev. Dyn. *239*, 2714–2721.

Little, S.C., Sinsimer, K.S., Lee, J.J., Wieschaus, E.F., and Gavis, E.R. (2015). Independent and coordinate trafficking of single Drosophila germ plasm mRNAs. Nat. Cell Biol. *17*, 558–568.

Van Der Maaten, L.J.P., and Hinton, G.E. (2008). Visualizing high-dimensional data using t-sne. J. Mach. Learn. Res. *9*, 2579–2605.

Marlow, F.L., and Mullins, M.C. (2008). Bucky ball functions in Balbiani body assembly and animal-vegetal polarity in the oocyte and follicle cell layer in zebrafish. Dev. Biol. *321*, 40–50.

Minshall, N., Reiter, M.H., Weil, D., and Standart, N. (2007). CPEB interacts with an ovary-specific eIF4E and 4E-T in early Xenopus oocytes. J. Biol. Chem. *282*, 37389–37401.

Nelson, M.R., Leidal, A.M., and Smibert, C.A. (2004). Drosophila Cup is an eIF4E-binding protein that functions in Smaug-mediated translational repression. EMBO J. *23*, 150–159.

Nishida, K.M., Okada, T.N., Kawamura, T., Mituyama, T., Kawamura, Y., Inagaki, S., Huang, H., Chen, D., Kodama, T., Siomi, H., et al. (2009). Functional involvement of Tudor and dPRMT5 in the piRNA processing pathway in Drosophila germlines. EMBO J. *28*, 3820–3831.

Nott, T.J., Petsalaki, E., Farber, P., Jervis, D., Fussner, E., Plochowietz, A., Craggs, T.D., Bazett-Jones, D.P., Pawson, T., Forman-Kay, J.D., et al. (2015). Phase transition of a disordered nuage protein generates environmentally responsive membraneless organelles. Mol. Cell *57*, 936–947.

Owens, D.A., Butler, A.M., Aguero, T.H., Newman, K.M., Van Booven, D., and King, M.L. (2017). High-throughput analysis reveals novel maternal germline RNAs crucial for primordial germ cell preservation and proper migration. Development *144*, 292–304.

Patel, A., Lee, H.O., Jawerth, L., Maharana, S., Jahnel, M., Hein, M.Y., Stoynov, S., Mahamid, J., Saha, S., Franzmann, T.M., et al. (2015). A liquid-to-solid phase transition of the ALS protein FUS accelerated by disease mutation. Cell *162*, 1066–1077.

Phillips, C.M., Montgomery, T.A., Breen, P.C., and Ruvkun, G. (2012). MUT-16 promotes formation of perinuclear Mutator foci required for RNA silencing in the C. elegans germline. Genes Dev. *26*, 1433–1444.

Prusiner, S.B. (1998). Prions. Proc. Natl. Acad. Sci. USA *95*, 13363–13383.

Raz, E. (2003). Primordial germ-cell development: the zebrafish perspective. Nat. Rev. Genet. *4*, 690–700.

Riemer, S., Bontems, F., Krishnakumar, P., Gömann, J., and Dosch, R. (2015). A functional Bucky ball-GFP transgene visualizes germ plasm in living zebrafish. Gene Expr. Patterns *18*, 44–52.

Shevchenko, A., Tomas, H., Havlis, J., Olsen, J.V., and Mann, M. (2006). In-gel digestion for mass spectrometric characterization of proteins and proteomes. Nat. Protoc. *1*, 2856–2860.

Shin, Y., and Brangwynne, C.P. (2017). Liquid phase condensation in cell physiology and disease. Science *357*, eaaf4382.

Shorter, J., and Lindquist, S. (2005). Prions as adaptive conduits of memory and inheritance. Nat. Rev. Genet. *6*, 435–450.

Siddiqui, N.U., Li, X., Luo, H., Karaiskakis, A., Hou, H., Kislinger, T., Westwood, J.T., Morris, Q., and Lipshitz, H.D. (2012). Genome-wide analysis of the maternal-to-zygotic transition in Drosophila primordial germ cells. Genome Biol. *13*, R11.

Siomi, M.C., Mannen, T., and Siomi, H. (2010). How does the royal family of Tudor rule the piwi-interacting RNA pathway? Genes Dev. *24*, 636–646.

Slaidina, M., and Lehmann, R. (2017). Quantitative differences in a single maternal factor determine survival probabilities among drosophila germ cells. Curr. Biol. *27*, 291–297.

Strasser, M.J., Mackenzie, N.C., Dumstrei, K., Nakkrasae, L.-I.I., Stebler, J., and Raz, E. (2008). Control over the morphology and segregation of zebrafish germ cell granules during embryonic development. BMC Dev. Biol. *8*, 58.

Takahashi, K., and Yamanaka, S. (2006). Induction of pluripotent stem cells from mouse embryonic and adult fibroblast cultures by defined factors. Cell *126*, 663–676.

Thandapani, P., O'Connor, T.R., Bailey, T.L., and Richard, S. (2013). Defining the RGG/RG motif. Mol. Cell *50*, 613–623.

Thomson, T., and Lasko, P. (2004). Drosophila Tudor is essential for polar granule assembly and pole cell specification, but not for posterior patterning. Genesis *40*, 164–170.

Tinevez, J.Y., Perry, N., Schindelin, J., Hoopes, G.M., Reynolds, G.D., Laplantine, E., Bednarek, S.Y., Shorte, S.L., and Eliceiri, K.W. (2017). TrackMate: an open and extensible platform for single-particle tracking. Methods *115*, 80–90.

Trapnell, C., Pachter, L., and Salzberg, S.L. (2009). TopHat: discovering splice junctions with RNA-Seq. Bioinformatics *25*, 1105–1111.

Trcek, T., Grosch, M., York, A., Shroff, H., Lionnet, T., and Lehmann, R. (2015). Drosophila germ granules are structured and contain homotypic mRNA clusters. Nat. Commun. *6*, 7962.

Tzung, K.W., Goto, R., Saju, J.M., Sreenivasan, R., Saito, T., Arai, K., Yamaha, E., Hossain, M.S., Calvert, M.E.K., and Orbán, L. (2015). Early depletion of primordial germ cells in zebrafish promotes testis formation. Stem Cell Reports *4*, 61–73.

Vasileva, A., Tiedau, D., Firooznia, A., Müller-Reichert, T., and Jessberger, R. (2009). Tdrd6 is required for spermiogenesis, chromatoid body architecture, and regulation of miRNA expression. Curr. Biol. *19*, 630–639.

Vourekas, A., Alexiou, P., Vrettos, N., Maragkakis, M., and Mourelatos, Z. (2016). Sequence-dependent but not sequence-specific piRNA adhesion traps mRNAs to the germ plasm. Nature *531*, 390–394.

Wang, H., Teng, Y., Xie, Y., Wang, B., Leng, Y., Shu, H., and Deng, F. (2013). Characterization of the carbonic anhydrases 15b expressed in PGCs during early zebrafish development. Theriogenology *79*, 443–452.

Wang, J.T., Smith, J., Chen, B.C., Schmidt, H., Rasoloson, D., Paix, A., Lambrus, B.G., Calidas, D., Betzig, E., and Seydoux, G. (2014). Regulation of RNA granule dynamics by phosphorylation of serine-rich, intrinsically disordered proteins in C. elegans. Elife *3*, e04591.

Weidinger, G., Stebler, J., Slanchev, K., Dumstrei, K., Wise, C., Lovell-Badge, R., Thisse, C., Thisse, B., and Raz, E. (2003). Dead end, a novel vertebrate germ plasm component, is required for zebrafish primordial germ cell migration and survival. Curr. Biol. *13*, 1429–1434.

Westerfield, M. (1995). The Zebrafish Book. A Guide for the Laboratory Use of Zebrafish (Danio rerio), Third Edition (University Oregon Press).

Wienholds, E. (2002). Target-selected inactivation of the zebrafish rag1 gene. Science *297*, 99–102.

Woodruff, J.B., Ferreira Gomes, B., Widlund, P.O., Mahamid, J., Honigmann, A., and Hyman, A.A. (2017). The centrosome is a selective condensate that nucleates microtubules by concentrating tubulin. Cell *169*, 1066–1077.e10.

Xiol, J., Cora, E., Koglgruber, R., Chuma, S., Subramanian, S., Hosokawa, M., Reuter, M., Yang, Z., Berninger, P., Palencia, A., et al. (2012). A role for Fkbp6 and the chaperone machinery in piRNA amplification and transposon silencing. Mol. Cell *47*, 970–979.

Yoon, C., Kawakami, K., and Hopkins, N. (1997). Zebrafish vasa homologue RNA is localized to the cleavage planes of 2- and 4-cell-stage embryos and is expressed in the primordial germ cells. Development *124*, 3157–3165.

STAR★METHODS

KEY RESOURCES TABLE

REAGENT or RESOURCE	SOURCE	IDENTIFIER
Antibodies		
Rabbit polyclonal anti-Tdrd6a	This paper Eurogentec	Epitope: QAVVHEPESEKEKRD
Rat polyclonal anti-Ziwi	This paper Eurogentec	Epitope: QLVGRGRQKPAPGAM
Rabbit polyclonal anti-Zili	Houwing et al. (2007)	N/A
Rabbit polyclonal anti-Tdrd1	Huang et al. (2011)	N/A
Sh-anti-DIG	Roche	Cat# 11333089001; RRID: AB_514496
Ms-anti-GFP (B-2)	Santa Cruz	Cat# Sc9996; RRID: AB_627695
Anti-Rb-Alexa405	Abcam	Cat# ab175651
Anti-Rb-Alexa647	Abcam	Cat# ab150075
Anti-Rt-Alexa488	Abcam	Cat# ab150153
Anti-Sh-Alexa555	Invitrogen	Cat# A21436; RRID: AB_2535857
Anti-Rb-IRDye	LI-COR	Cat# 926-32211; RRID: AB_621843
Anti-Rt-IRDye	LI-COR	Cat# 926-68076; RRID: AB_10956590
Anti-Ms-IRDye	LI-COR	Cat# 926-68070; RRID: AB_10956588
Anti-Ms-HRP	Cell Signaling Technology	Cat# 7076; RRID: AB_330924
Anti-Rb-HRP	Cell Signaling Technology	Cat# 7074; RRID: AB_2099233
Anti-DIG-AP Fab fragments	Roche	Cat# 11093274910; RRID: AB_514497
Chemicals, Peptides, and Recombinant Proteins		
Buc_R1	Peptide Specialty Laboratories GmbH	Biotin – ETEFTYCQ(sDMA)GRGSMKKRGSRY – $CONH_2$
Buc_R2	Peptide Specialty Laboratories GmbH	Biotin – ETEFTYCQRG(sDMA)GSMKKRGSRY – $CONH_2$
Buc_R3	Peptide Specialty Laboratories GmbH	Biotin – ETEFTYCQRGRGSMKK(sDMA)GSRY – $CONH_2$
Buc_R12	Peptide Specialty Laboratories GmbH	Biotin – ETEFTYCQ(sDMA)G(sDMA)GSMKKRGSRY – $CONH_2$
Buc_Cterm	Peptide Specialty Laboratories GmbH	Biotin – ETEFTYCQ(sDMA)G(sDMA)GSMKK(sDMA)GSRY – $CONH_2$
Ziwi_4	Peptide Specialty Laboratories GmbH	H2N-MTG(sDMA)ARARSRGRGRGQEP(BiotinC6) - $CONH_2$
Ziwi_47	Peptide Specialty Laboratories GmbH	Biotin - EGQLVG(sDMA)GRQKPAPGAMS - $CONH_2$
Ziwi_77	Peptide Specialty Laboratories GmbH	Biotin - KIGE(sDMA)GGRRRDFHDSG - $CONH_2$
Zili_228	Peptide Specialty Laboratories GmbH	H2N - G(sDMA)GFTGFGRAAMPHMTVK(BiotinC6) - $CONH_2$
XVelo	Peptide Specialty Laboratories GmbH	Biotin - RSFLY(sDMA)GHGLQK(sDMA)GTKKKGLN - $CONH_2$
TRIzol	Thermo Fisher	Cat# 15596018
TRIzol LS	Thermo Fisher	Cat# 10296010
TrypLE Express (1x)	Life Technologies	Cat# 12605036
Pronase	Sigma-Aldrich	Cat# P5147
MOPS buffer	Thermo Fisher	Cat# NP0001
4%-12% NuPage NOVEX gradient gel	Thermo Fisher	Cat# NP0321
NuPAGE LDS sample buffer 4x	Thermo Fisher	Cat# NP0007
Paraformaldehyde	Sigma-Aldrich	Cat# 441244
PBS	Gibco	Cat# 14190-094

(*Continued on next page*)

Continued

REAGENT or RESOURCE	SOURCE	IDENTIFIER
Immobilon-FL PVDF membrane	Merck	Cat# IPFL00010
Osmium Tetroxide, crystalline, highest Purity 99,95%	ScienceService	Cat# E19120
EMbed-812 Kit with DMP	ScienceService	Cat# E14120-DMP
Glutaraldehyde, 25% aqueous solution, EM grade	ScienceService	Cat# E16210
Paraformaldehyde, 20% aqueous solution, EM grade	ScienceService	Cat# E15713
Sodium cacodylate trihydrate	Sigma-Aldrich	Cat# 20840
4-Nitro blue tetrazolium chloride (NBT)	Roche	Cat# 11383213001
5-Bromo-4-chloro-3-indolyl phosphate (BCIP)	Roche	Cat# 11383221001
Yeast RNA	Sigma-Aldrich	Cat# R6625
Heparin	Sigma-Aldrich	Cat# H4784
Bovine Serum Albumin	Sigma-Aldrich	Cat# A7906
Dextran sulfate	Sigma-Aldrich	Cat# 42867-5G
Vanadyl-ribonucleoside complex	NEB	Cat# S1402S
ProLong™ Gold Antifade Mountant	Thermo Fisher	Cat# P10144
Formamide	Ambion	Cat# AM9342
Triton-X100	Sigma-Aldrich	Cat# T8787
Tween20	Sigma-Aldrich	Cat# P1379
cOmplete Mini, EDTA-free protease inhibitor cocktail Tablets	Roche	Cat# 11836170001
Dynabeads protein G	Invitrogen	Cat# 10004D
Streptavidin magnetic beads	Thermo Fisher	Cat# 65001
Glycoblue	Invitrogen	Cat# AM9515
Acetonitrile	Sigma-Aldrich	Cat# 271004
ReproSil-Pur 120 C18-AQ 1.9μm	Dr. Maisch GmbH	Cat# r119.aq.
Rhodamine B Dextran	Sigma-Aldrich	Cat# R9379-100MG
DIG labelling mix	Merck	Cat# 11277073910
IPL-41 insect medium	Gibco	Cat# 11405057
8-well μ-slides	ibidi	Cat# 80826
9μl X-tremeGENE™ HP	Roche	Cat# 6365779001
DpnI	New England Biolabs	Cat# R0176L
BP clonase II	Thermo Fisher	Cat# 11789020
LR clonase II plus	Thermo Fisher	Cat# 12538120
GFP-Trap Agarose	Chromotek	Cat# gta-100
Critical Commercial Assays		
Sp6 mMESSAGE MACHINE kit	Invitrogen	Cat# AM1340
Poly(A) tailing kit	Invitrogen	Cat# AM1350
Bioanalyzer Small RNA assay	Agilent	Cat# 5067-1548
Bioanalyzer High Sensitivity DNA assay	Agilent	Cat# 5067-4626
NEBNext® Small RNA Library Prep Set for Illumina	New England Biolabs	Cat# E7330
DNA 300 assay kit for Labchip XT	Caliper	Cat# PN 760601
Qubit dsDNA HS Assay	Life Technologies	Cat# Q32851
M-MLV reverse transcriptase, RNase H point mutant	Promega	Cat# M3681
iQ SYBR Green supermix	BioRad	Cat# 1708880
QIAquick PCR Purification Kit	Qiagen	Cat# 28106

(*Continued on next page*)

Continued

REAGENT or RESOURCE	SOURCE	IDENTIFIER
Ovation RNA-seq System V2	NuGEN	Cat# 7102
TruSeq DNA Sample Prep Kit	Illumina	Cat# 15026486
Deposited Data		
Raw and processed RNA-seq data	This paper	GEO: GSE79285
Mass spectrometry data	This paper	ProteomeXchange ID: PXD008322
Danio rerio (Zebrafish), Zv9 (GCA_000002035.2)	Zebrafish genome project	https://support.illumina.com/sequencing/sequencing_software/igenome.html
Uniprot/Trembl Danio rerio fasta	The UniProt Consortium	www.uniprot.org
smFISH probes	This paper; Mendeley Data	https://doi.org/10.17632/f9ckhbrvpd.1
Raw Confocal, Western blot and EM data	This paper; Mendeley Data	https://doi.org/10.17632/f9ckhbrvpd.1
Experimental Models: Cell Lines		
BmN4	Laboratory of Ramesh Pillai, Université de Genève	Bombyx mori ovary derived cell line
Experimental Models: Organisms/Strains		
Zebrafish:*tdrd6a*^{Q185}	This paper	N/A
Zebrafish:*buc*^{p106}	Bontems et al. (2009)	N/A
Zebrafish: *Tg(buc:buc-RtoK-egfp)*	This paper	N/A
Zebrafish: *Tg(buc:buc-wt-egfp)*	Riemer et al. (2015)	N/A
Zebrafish: *Tg(ziwi:tdrd6a-mcherry-polyA)*	This paper	N/A
Zebrafish: *Tg(kop:egfp-f-nos1-3'UTR)*	Köprunner et al. (2001)	N/A
Zebrafish: Tg(*vasa:egfp*)	Krøvel and Olsen (2002)	N/A
Oligonucleotides		
Fus_MO	GeneTools	GCCCATAATGATTTCACGGCATCTT
hook2_MO	GeneTools	GCTGATGTTTATTCAGGCTCATGGT
Tdrd6aQ185seq _F	N/A	GCCAATGCCTTACCACTATC
Tdrd6aQ185seq_genotype_R	N/A	CACTTGCCTCTGAATTCTTC
bucp106seq_F	N/A	TCTCCCCAAAGGGAGAACTCCATTG
bucp106seq_R	Sequence without transgene	GTTTAACATTTTAAACTGCTCAACATACCTCTG
Bucp106seqUTR_R	Sequence in presence of transgene	GTG TCC ATG TGT ACA TTT ATA GTG AAG TGC
hook2_mismatch_SP6_F	N/A	CATACGATTTAGGTGACACTATAGACAATGTCTTTAAACAAG CACCAACTGAGCGACTCTTTATTTATCTGGCTG
hook2_R	N/A	TCA TCG GGG CTG CAG GCG
Tdrd6a_attF	N/A	GGGG ACAAGTTTGTACAAAAAAGCAGGCT CCACC ATG TGC TCC ATT CCG GGA CTC CC
Tdrd6a_attR	N/A	GGGG AC CAC TTT GTA CAA GAA AGC TGG GTG ATC ACG CTT TTC TTT TTC ACT CTC GG
RtoKmut_GFPstart_F	N/A	P-GGCTCAAGATACGGCGGAAGCGGCATGGTGAGCAAG GGCGAGGAG
RtoKmut_R	N/A	CTT TTT CTT CAT AGA ACC TTT GCC CTT CTG GCA GTA GGC
BmDcp1 Fwd (BamHI)	N/A	AGT GGA TCC cAT GGC TGA CAC CGG GTT ACG
BmDcp1 Rev (NotI)	N/A	GGT GCG GCC GCT TAT GAC ACA GAA AAT GCT TTT TCT G
eGFP_F(BamHI)	N/A	AGT GGA TCC cAT GGT GAG CAA GGG CGA G
eGFP_R(BamHI)	N/A	GGT GGA TCC GCC TTG TAC AGC TCG TCC ATG CC
DrTdrd6a (NotI) Fwd	N/A	AGT GCG GCC GCC ATG TGC TCC ATT CCG GGA C
DrTdrd6a (XbaI) Rev	N/A	GGT TCT AGA CTA ATC ACG CTT TTC TTT TTC ACT C
Buc_F	N/A	P-GAAGGAATAAATAACAATTCACAACCAATGG

(*Continued on next page*)

Continued

REAGENT or RESOURCE	SOURCE	IDENTIFIER
Buc_R	N/A	GGG TAG GCC ATG GTG TAA GCT TG G TAT CTT GAG CCT CTT TTC TTC ATA GAA C
pBEMBL_R	N/A	GGC AGC CTC GAG CGG TGG
qpcr_nanos_F	N/A	GGCTTTTTCTCTTCTCCAATTCATCCTTTC
qpcr_nanos_R	N/A	GAGACTCCAGCAGCGCGGC
qpcr_dazl_F	N/A	CGGCGGTATTGATATGAAGGTGGATGAG
qpcr_dazl_R	N/A	GGAGATGACACTGACCGAGAACTTCG
qpcr_vasa_F	N/A	GGTCGTGGAAAGATTGGCCTG
qpcr_vasa_R	N/A	CAGCAGCCATTCTTTGAATATCTTC
qpcr_bactin_F	N/A	GACCCAGACATCAGGGAGTGATGG
qpcr_bactin_R	N/A	GGTCTCGAACATGATCTGTGTCATCTTC
Recombinant DNA		
pBEMBL-NHA-Buc-eGFP	This paper, backbone from Xiol et al. (2012)	N/A
pBEMBL-NHA-mCherry-DrTdrd6a	This paper, backbone from Xiol et al. (2012)	N/A
pBEMBL-NHA-mCherry-DCP1	This paper, backbone from Xiol et al. (2012)	N/A
pBEMBL-NHA-eGFP-DCP1	This paper, backbone from Xiol et al. (2012)	N/A
pME_tdrd6a	This paper	N/A
P5E_pziwi	Leu and Draper (2010)	N/A
P3E_mcherry-polyA	Tol2 kit	http://tol2kit.genetics.utah.edu/index.php/Main_Page
Tol2CG2	Tol2 kit	http://tol2kit.genetics.utah.edu/index.php/Main_Page
Tol2CG2_pziwi-tdrd6a-mcherrypA	This paper	N/A
Software and Algorithms		
MaxQuant v.1.5.2.8	Cox and Mann (2008)	http://www.coxdocs.org/doku.php?id=:maxquant:start
cutadapt	[https://doi.org/10.14806/ej.17.1.200]	https://cutadapt.readthedocs.io/
fastq *quality_filter*	N/A	http://hannonlab.cshl.edu/fastx_toolkit/
seqtk trimfq	N/A	https://github.com/lh3/seqtk
Bowtie v0.12.8	http://genomebiology.com/2009/10/3/R25	http://bowtie-bio.sourceforge.net/index.shtml
TopHat	Trapnell et al. (2009)	http://cole-trapnell-lab.github.io/projects/tophat/
DESeq	Anders and Huber (2010)	https://www.bioconductor.org/packages/release/bioc/html/DESeq.html
RaceID	Grün et al. (2015)	https://github.com/dgrun/RaceID
TrackMate	Tinevez et al. (2017)	https://github.com/fiji/TrackMate/releases/tag/TrackMate_-3.5.3

CONTACT FOR REAGENT AND RESOURCE SHARING

Further information and requests for resources and reagents should be directed to and will be fulfilled by the Lead Contact, René F. Ketting (r.ketting@imb.de).

EXPERIMENTAL MODEL AND SUBJECT DETAILS

Zebrafish Lines

Zebrafish strains were housed at the Institute of Molecular Biology in Mainz and bred and maintained under standard conditions (26-28°C room and water temperature and lighting conditions in cycles of 14:10 hours light:dark) as described by (Westerfield, 1995). Larvae < 5 days post fertilization were kept in E3 medium (5 mM NaCl, 0.17 mM KCl, 0.33 mM $CaCl_2$, 0.33 mM $MgSO_4$) at 28°C. The *tdrd6a*$^{Q185X/+}$ mutant allele zebrafish was derived from ENU mutagenized libraries using target-selected mutagenesis

as described before (Wienholds, 2002). Animals carrying *tdrd6a*$^{Q185X/+}$ were out crossed against wt fish (AB and Tue), and the following pre-existing lines: *kop:egfp-f-nos1-3'UTR*, *vasa:egfp* or *buc:buc-egfp-buc3'UTR* transgenic fish (Köprunner et al., 2001; Krøvel and Olsen, 2004; Riemer et al., 2015) and subsequently incrossed to obtain *tdrd6a*$^{Q185X/Q185X}$ offspring. All experiments were conducted according to the European animal welfare law and approved and licensed by the ministry of Rhineland-Palatinate.

Cell Culture

BmN4 cells were a kind donation of the laboratory of Ramesh Pillai. BmN4 cells were cultured at 27°C in IPL-41 (Gibco) medium supplemented with 10%FBS (Gibco) and 0.5% Pen-Strep.

METHOD DETAILS

Genotyping

For genotyping, the DNA was extracted form caudal fin tissue, amputated from anesthetized fish. The primers used to amplify and sequence the *tdrd6a*^{Q185} allele were Tdrd6aQ185seq_F: GCCAATGCCTTACCACTATC and Tdrd6aQ185seq_genotype_R CACTTGCCTCTGAATTCTTC. The lesion induces a truncation after amino acid Q185. This residue precedes the epitope used for immunization. The *buc*^{p106} allele was amplified with bucp106seq_F: TCT CCC CAA AGG GAG AAC TCC ATT G and bucp106seq_R: GTT TAA CAT TTT AAA CTG CTC AAC ATA CCT CTG and sequenced with the reverse oligo.

Tdrd6a Antibody

Tdrd6a antibodies were raised in rabbits with the synthetic peptide H_2N-QAVVHEPESEKEKRD-CONH$_2$. Antisera were subsequently purified against the synthetic peptide (Eurogentec).

Whole Mount Colorimetric In Situ Hybridization Embryos

Embryos were collected and fixed at 4-cell stage in 4% PFA/PBS ON at 4°C. Next, they were washed with PBST and dechorionated using forceps, followed by storage in MeOH at least ON at -20°C. Upon rehydration, embryos were blocked in Hyb+ (50% de-ionized formamide, 5xSSC, 0.1%Tween-20, 5mg/ml yeast RNA, 50μg/ml heparin) for 2 hrs at 70 °C. Next, samples were incubated ON at 70 °C with DIG-labelled probe in Hyb+. After probe removal, samples were washed at 70 °C: 2 x 20 minutes in Hyb- (Hyb+ without yeast RNA and heparin), 2 x 20 minutes in 2xSSCT, 2 x 20 minutes in 0.2xSSCT. Samples were washed twice in TBST at RT and blocked 1 hour in 10% BSA. Next, samples were incubated with 1:2000 anti-DIG-AP Fab fragments (Roche) in 10% BSA ON at 4°C. Next day, they were washed 3 x 20 min. in TBST at RT and 2 x 10 min. in AP-staining buffer (100mM NaCl, 100mM Tris pH9.5, 50mM $MgCl_2$, 0.1% Tween-20), followed by incubation with NBT (4.5μl/ml AP staining buffer; Roche) and BCIP (3.5μl/ml AP staining buffer; Roche) to stain the embryos.

Whole Mount Fluorescent In Situ Hybridization

Ovary tissue was put in OR2 medium (82mM NaCl, 2mM KCl, 1mM $MgCl_2$, 5mM HEPES pH7.5) and filtered through a 300μm mesh to collect only stage I-III oocytes. These oocytes were fixed in 4% PFA/PBS 3 hours at RT, followed by dehydration in MeOH and storage ON at -20°C. The same procedure was followed as described above for colorimetric ISH, only after blocking in 10% BSA, samples were incubated with 1:1000 sheep-anti-DIG (Roche) in 10% BSA ON at 4°C. After 3 x 20 min. washing in TBST, samples were incubated with 1:500 anti-sheep-Alexa555 (Invitrogen) for 1 hr/RT. Samples were washed 3 x 10 min. in TBST and mounted in 80% glycerol, followed by imaging under DM6000 Leica microscope.

Whole Mount Double smFISH and IHC

PFA fixed oocytes/embryos were collected and prepared as described above and were incubated overnight with 1:100 anti-Tdrd6a and 1:100 of both smFISH probes (Stellaris™ custom design, Quasar 570 (*vasa*) and Quasar 670 (*dazl*) labelled) stocks (12.5μM in TE buffer) in hybridization buffer (10% dextran sulfate, 10% formamide, 1mg/mL tRNA, 0.02%BSA, 2mM vanadyl-ribonucleoside complex (NEB S1402S) in 2xSSC) at 30°C. Next day, wash 15 minutes in wash buffer (10% formamide, 2xSSC) and incubate in 1:500 anti-rabbit alexa-405 for 30 minutes in wash buffer. Then wash 2 x 15 minutes in wash buffer and mount in ProLong™ Gold Antifade Mountant (ThermoFisher).

Peptide Pull-Down

Peptides were synthesized by Peptide Specialty Laboratories GmbH. 20μg peptide in 500μL IP buffer (25 mM Tris pH 7.5, 150 mM NaCl, 1.5 mM $MgCl_2$, 1% Triton-X100, 1mM DTT, protease inhibitor) was pre-incubated with streptavidin-coupled magnetic beads for 30 minutes at RT, rotating. 20μL resin (ThermoFisher 65001) was used per pulldown. Then, the respective lysate was added to the washed beads and incubated for 1hr at 4°C while rotating. The beads were then washed with wash buffer (25mM Tris pH 7.5, 300mM NaCl, 1.5mM $MgCl_2$, 1mM DTT) and either used for Western blot analysis or MS.

FRAP

FRAP was performed on a TCS SP5 Leica confocal microscope, equipped with a FRAP-booster, using a 63x oil objective with an NA of 1.4 (BmN4 cells) or a 63x water objective with an NA of 1.2 (Bb). In BmN4 cells, entire granules were bleached in a fixed region of

1.5μm ø and recovery was followed for 1500 frames (0.2s/frame). Bbs were bleached partially in a fixed region of 2.5μm ø and recovery was followed for 1500 frames (0.5s/frame). Regions (pre– and post-bleach) were tracked using TrackMate (Tinevez et al., 2017). 10 pre-bleach frames were recorded and after background subtraction, the average intensity was used as pre-bleach intensity. Post-bleach frames were background subtracted and to make replicates comparable, post-bleach frame #1 of each measurement was set to 0 and corresponding pre-bleach intensity was corrected for this. Normalization of Buc-eGFP and mCherry-Tdrd6a was performed by plotting intensities of mCherry-eGFP using the same microscope settings as for the FRAP. Intensities were plotted after background subtraction and the resulting curve was used to calculate protein ratios using the initial/pre-bleach intensities of each experiment.

Immunohistochemistry

Samples were prepared as described for the ISH above and either embedded in paraffin and sectioned (ovary Figures 1A and S7A) or used whole mount. The samples were blocked in block buffer (2% sheep serum, 2%BSA in PBS with 0.05% Tween (PBST)) for 1 hour at RT and next incubated with the primary antibody in block buffer overnight at 4°C. The next day, samples were washed 3 x 5 minutes in PBST and incubated with the secondary antibody in block buffer for 1 hour at RT. The samples were washed 4 x 15 minutes in PBST and mounted in ProLong™ Gold Antifade Mountant prior to imaging. Rb-anti-Tdrd6a antibody was used 1:100, rat-anti-Ziwi was used 1:100. Anti-rabbit alexa-647 (Abcam, ab150075) and anti-rat alexa-488 (Abcam ab150153) was used 1:500.

Confocal Imaging

Samples were imaged using a TCS SP5 Leica confocal microscope using a 10x dry objective (NA 0.3), 40x oil (NA 1.3), 63x oil (NA of 1.4) or a 63x water objective (NA 1.2). The following figures were deconvolved using the Huygens software: Figures 3C, 3D, 4A, 4B, 6A, 6D, 7D, S1C, S4A, and S6A

Immunoprecipitation

Per IP the following amounts of sample was used: 2 testis lobes, stage I-III oocytes from 1 female or 40 1-cell stage embryos (remove all E3 prior to addition of lysis/IP buffer). Samples were taken up in 650 μL lysis/IP buffer (25 mM Tris pH 7.5, 150 mM NaCl, 1.5 mM $MgCl_2$, 1% Triton-X100, 1mM DTT, protease inhibitor) and homogenized with a micropestle followed by sonication for 3 x 30 seconds at low power. The oocyte and testis samples were spun down 10 minutes at 12,000 x g at 4°C and the supernatant was used for IP. The embryo samples were filtered through a 70 micron mesh to remove the chorion fragments and the filtrate was used for IP directly. The Tdrd6a antibody was used at a dilution of 1 to 100 and incubated for 2 hours at 4°C while rotating. Then 30 μl washed Dynabeads protein G were added and incubated with the sample for another 45 minutes at 4°C. Next, 3 washes were performed with wash buffer (25 mM Tris pH 7.5, 300 mM NaCl, 1.5 mM $MgCl_2$, 1mM DTT). For pulldown of the GFP-tagged constructs, 25μl GFP-Trap (GFP-Trap_A, Chromotek) per lysate was used and incubated for 1 hour at 4°C, followed by 3 washes with wash buffer.

For q-RT-PCR and RIP-seq analysis, Dynabeads were eluted in TRIzol LS (ThermoFisher) for RNA isolation. For western blot and mass spectrometry analysis, Dynabeads or GFP-Trap beads were eluted in NuPAGE LDS sample buffer (ThermoFisher).

Western Blot

Samples were heated to 95°C for 5 minutes prior to loading on a 4%-12% NuPage NOVEX gradient gel (ThermoFisher) and blotted on an Immobilon-FL PVDF membrane (Merck) overnight at 15V, RT. The membranes were incubated next day with primary antibodies (Rb-α-Tdrd6a 1:1000, Rt-α-Ziwi 1:1000, Rb-α-Tdrd1 1:500, Rb-α-Zili 1:10,000, Ms-α-GFP (Santa Cruz) 1:1000) and upon washing incubated with 1:10,000 800CW IRDye α-Rb and IRDye 680RD α-Rt (LI-COR) and imaged on an Odyssey CLx imaging system (LI-COR).

Library Construction and High-Throughput Sequencing

Total RNA was subjected to 15% TBE-urea gel for size selection of 15– 35 nt. This excised gel fraction was eluted in 0.3 M NaCl for N16 h and precipitated with 100% isopropanol and Glycoblue for 1h at −20 °C. The precipitated RNA pellet was washed once with 75% ethanol and dis- solved in nuclease-free water. The purified RNA fraction was confirmed by Bioanalyzer Small RNA assay (Agilent). Library preparation was based on the NEBNext® Small RNA Library Prep Set for Illumina® (New England Biolabs) with minor modifications. To counteract ligation bias and to remove PCR duplicates, small RNA was first ligated to the 3′ adapter and then the 5′ adapter, both of which contained four random bases at the 5′ and 3′ end, respectively. Adapters with random bases were chemically synthesized by Bioo Scientific. Adapter-ligated RNA was reverse-transcribed and PCR amplified for 14 cycles using index primers. The PCR amplified cDNA construct was checked on the Bioanalyzer (Agilent) using High Sensitivity DNA assay. We performed a size selection of the small RNA library on LabChip XT instrument (PerkinElmer) using the DNA 300 assay kit. All libraries were pooled to obtain 10 nM, which was denatured to 9 or 10 pmol with 5% PhiX spiked-in and sequenced as single-read for 50 cycles on an Illumina MiSeq or HiSeq 2500 instrument in either rapid or high-output mode.

Bioinformatic Analysis

The quality of raw sequenced reads was accessed with FastQC, Illumina adapters were then removed with cutadapt (-O 8 -m 26 -M 38), reads with low-quality calls were filtered out with fastq quality_filter (-q 20 -p 100 -Q 33). Using information from unique molecule identifiers (UMIs) added during library preparation, reads with the same sequence (including UMIs) were collapsed to removed

putative PCR duplicates using a custom script. Prior to mapping, UMIs were trimmed (seqtk trimfq) and library quality re-assessed with FastQC. Reads were aligned against the Zebrafish (_Danio rerio) genome assembly Zv9 with bowtie v0.12.8 (—tryhard —best —strata —chunkmbs 256 -v 1 -M 5).

The locations of transposable elements were downloaded from the UCSC genome browser (repeat masker track, Zv9) and used to select reads reads mapping to either RNA (SINE, LINE and LTR) or DNA transposons. The strength of the ping-pong cycle was assessed as the 5' overlap of reads in opposite strands (Brennecke et al., 2007) and the Z-scores scores were calculated as Z-score = (P10-M)/SD, where P10 is the number of read pairs with an offset of 10 bases, M the mean of read pairs with 1-9 and 11-30 bases, and SD the standard deviation.

LC-MS/MS

Mass Spectrometry Sample Preparation

Proteins were heated to 80°C for 10 min prior to loading on a 4%-12% NuPage NOVEX gradient gel (Life Technologies). The proteins were separated using MOPS buffer (ThermoFisher) at 170V for 10 min. In-gel digestion was performed essentially as previously described (Shevchenko et al., 2006). Peptides were desalted on StageTips and stored on them until MS measurement.

Mass Spectrometry Measurement

Peptides were eluted from StageTips with 80 percent ACN/0.5% formic acid. The mixture was separated using an EASY-nLC1000 with a reversed phase column (25 cm, 75 μm inner diameter, packed in-house with ReproSil-Pur C18-AQ 1.9 μm (Dr. Maisch GmbH)) mounted directly at a Q Exactive Plus mass spectrometer (ThermoFisher). A 88 minute gradient of 2% to 40% acetonitrile at a flow of 225 nl/min was combined with a wash-out of 95% acetonitrile in an overall 105 min instrument method. Spray voltage was set to ca. 2.4 kV. The instrument performed a top10 data-dependent acquisition with up to 10 HCD fragmentations per MS full scan (70k resolution, 300-1650 m/z).

MS Analysis

The raw files were processed with MaxQuant v.1.5.2.8 and searched with the incorporated Andromeda search engine against a Uniprot/Trembl Danio rerio fasta file (58,793 entries) (Cox and Mann, 2008). Carbamidomethylation was set as fixed modification while methionine oxidation, protein N-acetylation, phosphorylation and lysine/arginine dimethylation were considered as variable modifications. The search was performed with an initial mass tolerance of 7ppm mass accuracy for the precursor and 20 ppm for the MS/MS spectra in the HCD fragmentation mode. Standard settings were applied except match between runs and the LFQ quantitations were activated. Search results were filtered at a false discovery rate of 0.01 on protein and peptide level.

Data Analysis

For statistical analysis of the MS data, protein groups identified by site, known contaminants and reverse hits were excluded. The dataset was further filtered for at least 2 peptide identifications (at least 1 unique and 1 razor) per protein group. Missing LFQ values were imputed using lower values of a beta distribution derived from the measured values. Provided LFQ values were $\log_2$ transformed and for the volcano plot, the mean of the LFQ intensity of the Tdrd6a IP subtracted with the mean of the LFQ intensity of IgG IP (x-axis) against the p-value from a Welch t-test between both groups (y-axis) were plotted.

Fluorescence-Activated Cell Sorting (FACS)

Embryos were collected at the stage of interest in 20 ml E3 medium (5 mM NaCl, 0.17 mM KCl, 0.33 mM $CaCl_2$, 0.33 mM $MgSO_4$) in a glass beaker. 500μl 10mg/ml pronase was added to remove the chorions. The chorions were washed away with E3 and the embryos were taken up in 1 mL TrypLE Express (1x) (Life Technologies) and dissociated with the help of a syringe. The samples were added to 6 mL E3, 5 μL 1M EDTA and 0.5 mL FCS was added. Samples were centrifuged for 5 minutes at 1000g. Supernatant was removed and cells were taken up in PBS. Cells were pipetted through a cell strainer and 10 μL Dnase was added. Prior to sorting, DAPI was added. Single GFP-positive cells were sorted using a BD FACSAria III (Becton Dickinson) with an 85 μm nozzle in 96 well plates containing 150 μL TRIzol Reagent (ThermoFisher).

CEL-Seq Library Preparation

After sorting, single cell TRIzol extractions were performed and the dried RNA pellet was resuspended in primer solution, containing the 5' Illumina adapter, a cell specific barcode, a unique molecular identifier (UMI), the T7 promoter and a poly T stretch. The RNA-primer solution was briefly denatured, cooled on ice and subsequently first strand synthesis mix was added. After the first strand synthesis reaction the DNA:RNA hybrids were converted into dsDNA, cleaned up and subsequently o/n *in vitro* transcription was performed. The obtained RNA was thereafter fragmented and Illumina compatible libraries were made using the TruSeq small RNA sample prep kit. (Grün et al., 2014).

Quantification of Transcript Abundance

Paired end read processing obtained by CEL-Seq was essentially done as described with minor modifications (Grün et al., 2015). The transcriptome of all Ensembl genes (version Zv9) was downloaded and all isoforms were merged into single genes. We aligned the reads with BWA using standard settings to the improved Ensembl transcriptome as described (Junker et al., 2014). The right read was mapped to the gene models whereas the left mate, containing the UMI, was used for quantification. Barcode frequencies were converted based on binominal statistics into transcript count.

RaceID2

RaceID2 was used with default settings. The lower limit of transcript counts per cell we used was 1100 transcripts per cell. Thereafter the transcript counts of all cells passing this threshold were down sampled to 1100 transcripts per cell. The data described in Figures S3I and S3J was obtained from cells down sampled to 1750 transcripts to be able to pick up more lowly expressed genes as well. K-medoids clustering was performed similarly as the k-means clustering as described (Grün et al., 2015), but optimal cluster number was not determined by gap statistics, but by determining the saturation point of the within cluster dispersion (Grün et al., 2016). For t-SNE-map generation a seed of 2500 was used. Standard deviations on the individual Gp correlations were obtained by bootstrapping (n=100).

Detection of Differentially Expressed Genes in scRNA-Seq Data

To identify differentially expressed genes we applied an approach akin to previously published method (Anders and Huber, 2010). First, the down-sampled version computed by RaceID2 was used as input, in order to compare two subsets of cells from the same dataset. A p-value for a significant difference in mean expression of a gene between the two subsets was computed using DESeq as described in (Anders and Huber, 2010) while using the RaceID background model (Grün et al., 2015) to estimate the dispersion parameter of the negative binomial expression distribution within the two subgroups. These p-values were corrected for multiple testing by the Benjamini-Hochberg method.

Background Correlation Model and Random Cell Generation

To compute the expected Spearman correlations values of transcripts with a particular average expression we ranked the genes in our dataset according to their average expression. For every Gp pair for which we computed the pairwise correlation we took the three genes above and below the two Gp genes in question from the ranked list and computed all their pairwise correlations. The pairwise correlation between Gp markers was done with all cells at 3.5hpf except one, which was discarded after manually checking of atypical Gp expression levels. This particular cell expressed tdrd7 > 200-fold higher than the average cell in the 3.5hpf dataset and was considered a technical artifact.

Generation of random cell was done by randomly ascribing Gp counts derived from cells at the 3.5hpf timepoint and we subsequently computed the pairwise correlation of the Gp mRNAs in these hypothetical cells.

qPCR

From total RNA from input and Tdrd6a IP samples, cDNA was synthesized with M-MLV reverse transcriptase (RNase H point mutant, Promega), using random hexamers (Promega). qPCR was performed using iQ SYBR Green supermix (BioRad) on a CFX384 Real-Time thermal cycler (Bio Rad). All oligos were tested for linearity prior to the experiment.

RIP-Seq

RNA was isolated from input samples and Tdrd6a IP experiments on freshly laid embryos by TRIzol extraction according to manufacturer's instructions. 1.5 ng of immunoprecipitated or input material as total RNA was amplified to cDNA with Ovation RNA-seq System V2 (NuGEN) followed by purification with QIAquick PCR Purification Kit (Qiagen). The purified full-length cDNA was sheared to around 200 bp by a focused-ultrasonicator (Covaris). 1 μg of sheared cDNA was end-repaired and adapter-ligated following manufacture's instruction of TruSeq DNA Sample Prep Kit (Illumina). Size selection of adapter-ligated cDNA between 200-400 bp was done by LabChip XT (PerkinElmer). This size-selected fraction was PCR amplified for 3 cycles before pooling for paired-end sequencing on HiSeq 2500 for 50 bp read length. Around 30 million reads per sample were available for processing. Reads were aligned to Zv9 using TopHat with default settings. DESeq was used to compute significance of observed differences between Tdrd6a RIP and input counts per gene (Anders and Huber, 2010). Only genes with on average more than 50 RPM were used for further analysis.

Morpholino Knockdown and PGC Quantification

A morpholino was designed antisense to the region containing the start-codon of *hook2* (GeneTools). 1nl was injected into 1-cell stage *pvasa:egfp* positive embryos at a concentration of 0.5mM and co-injected with $1/10^{th}$ volume of rhodamine dextran. This was also performed using a morpholino targeting the *fus* transcript at the same concentration. Rescue experiments were performed by mixing 200ng/μL final concentration in the MO injection mix. *Hook2* mRNA was amplified using an oligo containing an Sp6 promoter and mismatches at the MO binding site. mRNA was synthesized using the Sp6 mMESSAGE MACHINE kit (Invitrogen), followed by poly-A-tailing using the poly(A) tailing kit (Invitrogen). At 24hpf, the larvae were dechorionated and fixed in 4%PFA/PBS so GFP positive PGCs could be counted at the same developmental stage. 1dpf, embryos were dechorionated and fixed in 4%PFA/PBS and observed through Leica stereo microscope for counting PGCs.

Electron Microscopy

Gonads of 5wpf Tdrd6a Mut and WT fish were fixed with half-strength Karnovsky fixative (pH 7.4, Karnovsky, 1965) and postfixed with 1% OsO4 in 0.1M Cacodylate buffer (pH7.4), dehydrated in an Acetone series and embedded in EPON (Karnovsky, 1965). Semi-thin sections (1.5μm) were cut on a Reichert Ultracut 2040 and a Butler diamond knife (Diatome) until the desired area in the

gonad was reached. Ultra-thin sections (90nm) were cut on a Reicher Ultracut E and collected on pioloform coated copper slot grids, dried and stained with leadcitrate under oxygen free conditions for 2 minutes. Sections were examined with a Zeiss LIBRA 120.

BmN4 Cell Transfection

For imaging of transfected BmN4 cells, cells were grown overnight in 8-well μ-slides (ibidi 80826). A total of 300ng construct mix (co-transfection 300ng total or single transfection 150ng plus 150ng empty vector) was incubated with 0.9μl X-tremeGENE™ HP (Roche) filled up to 30μL with insect medium without additives for 30 minutes prior to transfection.

Cloning

Tdrd6a-mCherry-polyA Construct

The transgene was made using Tol2 kit for multisite Gateway cloning. The *tdrd6a* CDS was amplified and cloned into pDonr221 using BP clonase in order to obtain pME_tdrd6a. Next, an LR reaction was performed using p5E_pziwi (ziwi promoter), pME_tdrd6a, p3E_mCherry-polyA and tol2CG2 (pDest) (Kwan et al., 2007; Leu and Draper, 2010). Injected embryos were screened for *cmlc2:gfp* to create a line. The expression pattern of this transgene was limited to oocytes up to stage Ib to early stage II (data not shown).

Buc-RtoK-eGFP Mutant Construct

The Buc construct used to make the Buc-eGFP line (Riemer et al., 2015) was modified with PCR in order to obtain the RtoK mutated version. First, the plasmid was digested with NotI and SalI and the resulting 4064 bp fragment was subcloned in pre-digested pCS2+. Arginine codons were replaced by Lysine codons using RtoKmut_GFPstart_F (phosphorylated): GGCTCA AGATACGGCGGA AGCGGCATGGTGAGCAAGGGCGAGGAG and RtoKmut_R: CTT TTT CTT CAT AGA ACC TTT GCC CTT CTG GCA GTA GGC. This also causes loss of intron 6, however, since the other introns remained unaffected and the transgene was translated and could localize normally in the presence of wt Buc, this does not seem to affect the functionality of the transgene. After the PCR, the original plasmid was digested with DpnI and the PCR fragment was circularized by ligation and sequenced. Next, the mutated fragment was ligated back into the pre-digested *buc-egfp* plasmid. The mutated construct was injected into wt embyros together with *tol2* transposase and adult females were screened for GFP-positive gonads. The F0 females were then outcrossed in order to obtain a stable line, prior to crossing it with the buc^{p106} allele.

Cloning of the BmN4 Expression Constructs

Dcp1 was amplified and digested with BamHI and NotI and ligated into pBEMBL-NHA. Next, mCherry and eGFP were amplified and ligated N-terminally into the BamHI site in order to create mCherry-Dcp1 and eGFP-DCP1 respectively. Tdrd6a was amplified and digested with NotI and XbaI and ligated into pre-digested pBEMBL-NHA-mCherry. Buc was amplified using Buc F, which was 5' phosphorylated, and Buc_R, containing an overhang for the pBEMBL-NHA-eGFP. Next, the amplicon was mixed with pBEMBL-NHA-eGFP and together with the pBEMBL_R oligo, a PCR was performed on the entire plasmid. Next, the original backbone was digested with DpnI and the linear PCR product was ligated (and thereby circularized) in order to obtain pBEMBL-NHA-Buc-eGFP.

QUANTIFICATION AND STATISTICAL ANALYSIS

Quantification of the fluorescent Western blot was done using the Image Studio software from LI-COR.

For the qPCR, standard deviations of 2 biological replicates of triplicate measurements were calculated. P-values were calculated using a two-sided Student's t-test on the ΔCt values.

The surface of the 2D information of the Buc granules in the BmN4 cells was calculated in Fiji. First, single plane confocal images (1 Airy unit) were binarised using the Otsu method. Next, the surface of the granules was measured using 'Analyze Particles' (size: > 0.1μm^2).

All p-values for the boxplots were calculated using the two-sided Wilcoxon test, in order to compare significant differences between two populations.

DATA AND SOFTWARE AVAILABILITY

Raw and processed RNA-seq data files have been deposited in the NCBI Gene Expression Omnibus (GEO) under the accession number GEO: GSE79285.

Mass spectrometry data has been submitted to ProteomeXchange: PXD0088322.

Developmental Cell, Volume *46*

Supplemental Information

Tdrd6a Regulates the Aggregation of Buc into Functional Subcellular Compartments that Drive Germ Cell Specification

Elke F. Roovers, Lucas J.T. Kaaij, Stefan Redl, Alfred W. Bronkhorst, Kay Wiebrands, António M. de Jesus Domingues, Hsin-Yi Huang, Chung-Ting Han, Stephan Riemer, Roland Dosch, Willi Salvenmoser, Dominic Grün, Falk Butter, Alexander van Oudenaarden, and René F. Ketting

Supplemental Figure 1

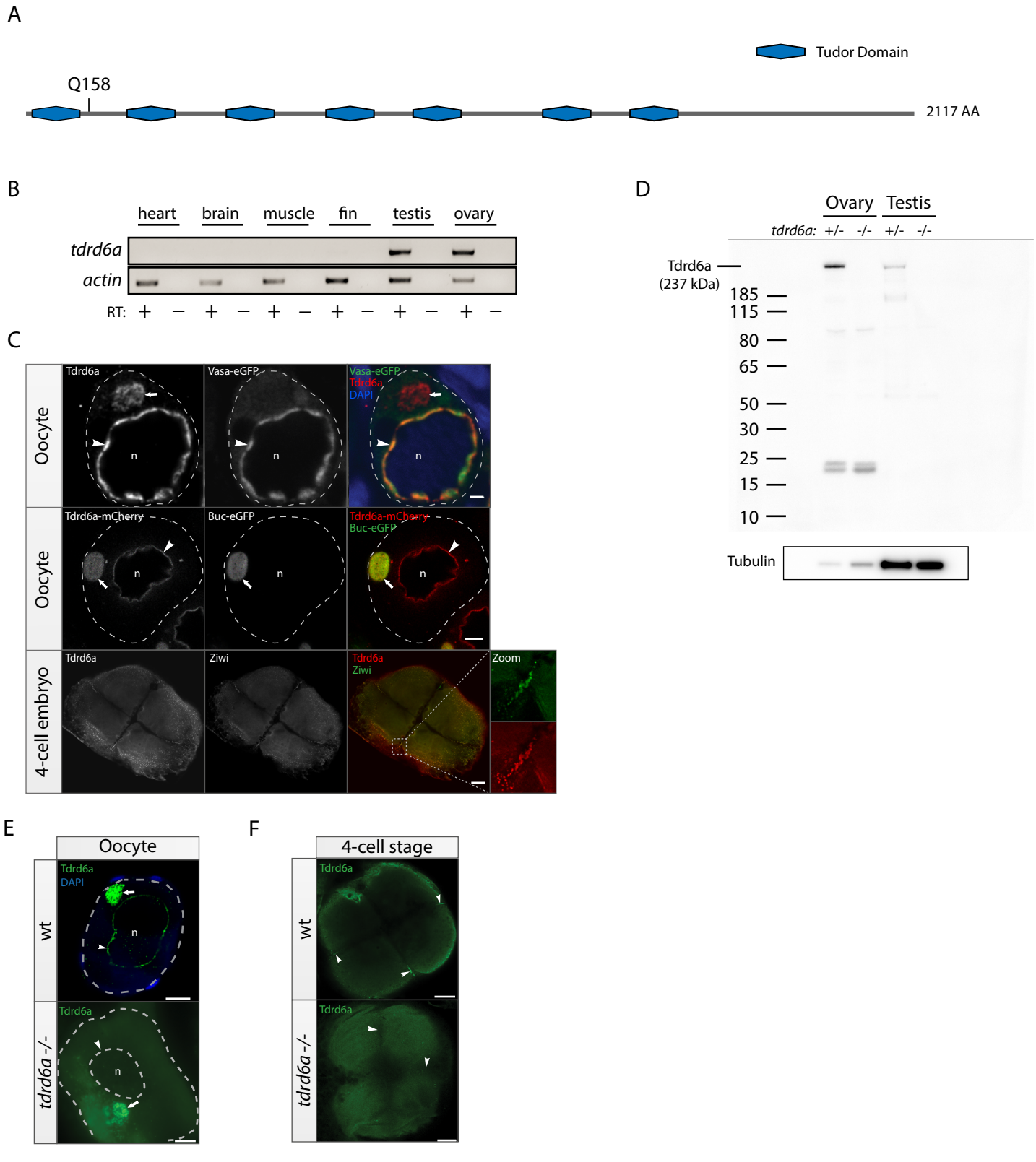

Supplemental Figure 2

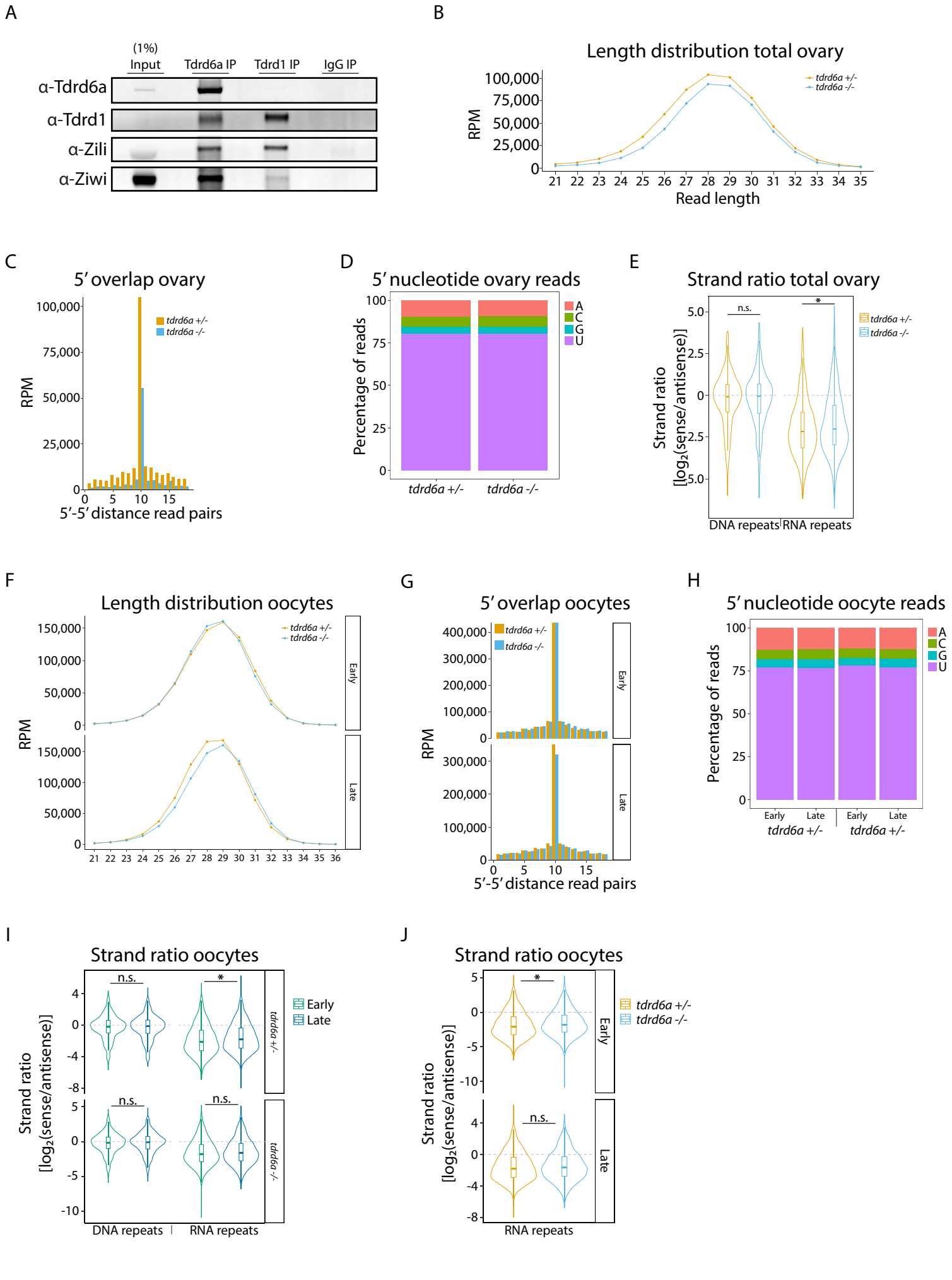

Supplemental Figure 3

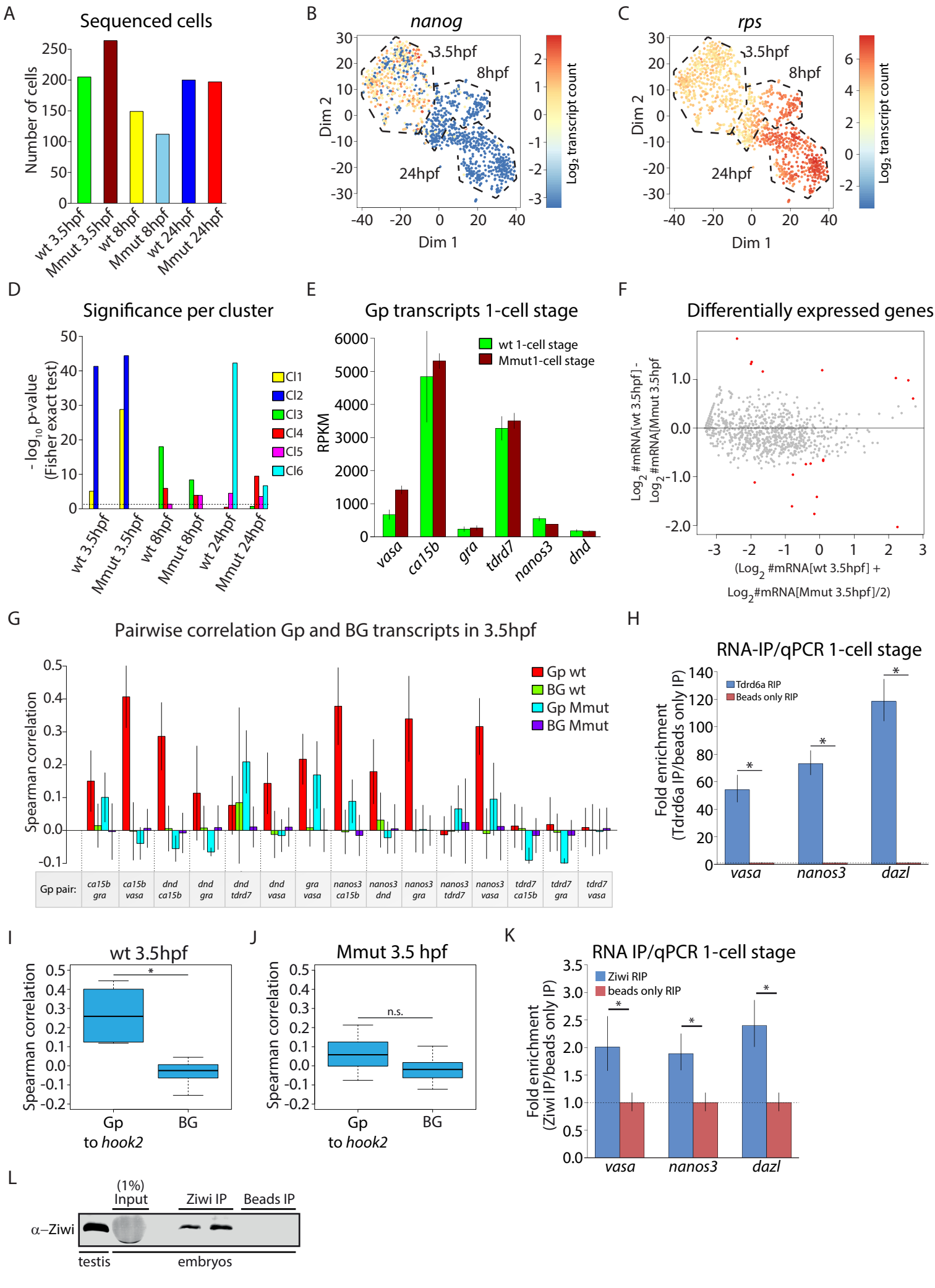

Supplemental Figure 4

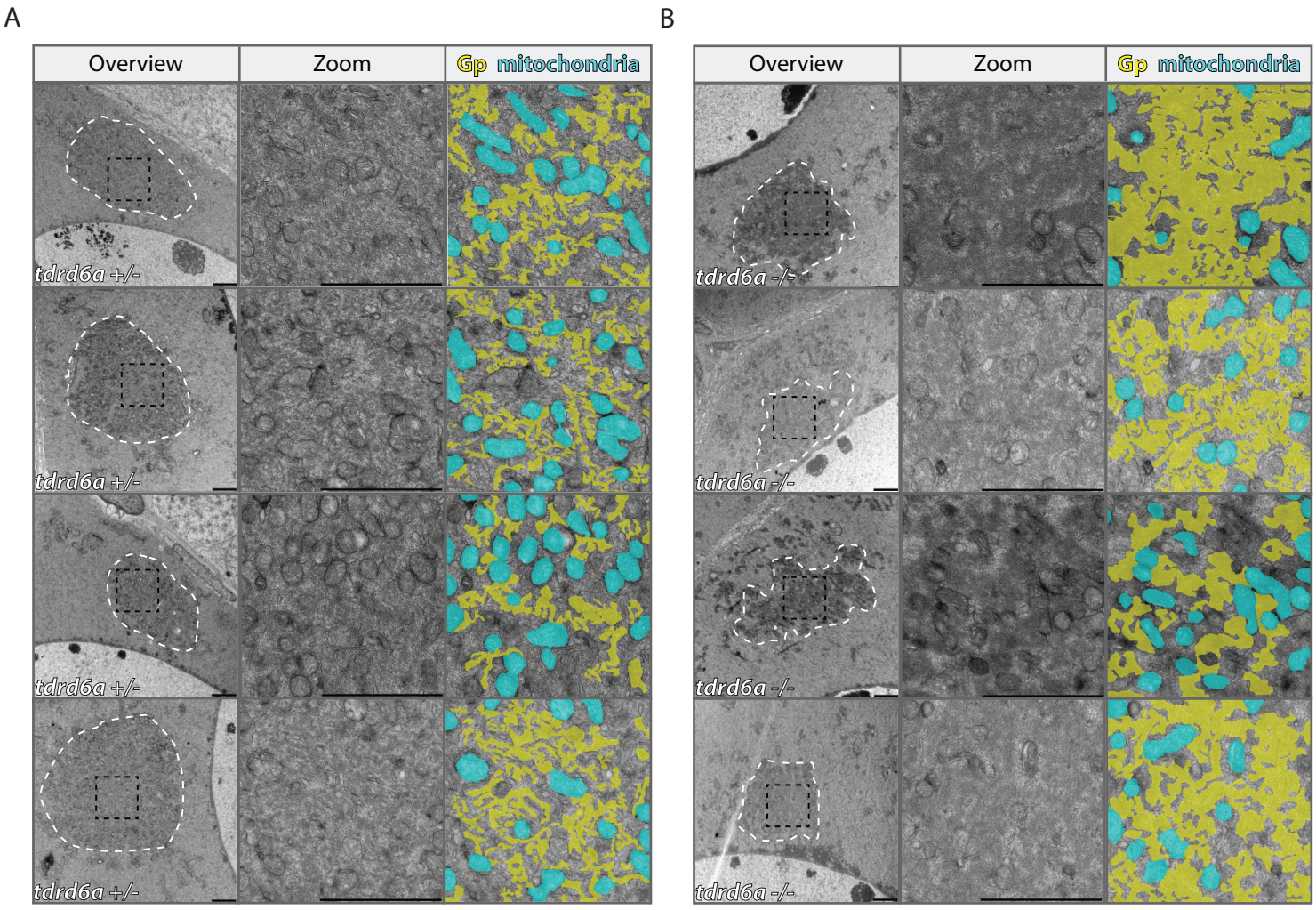

Supplemental Figure 5

A

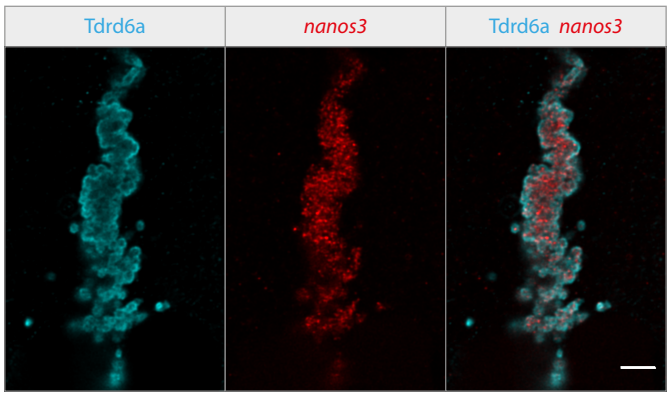

B

Supplemental Figure 6

A

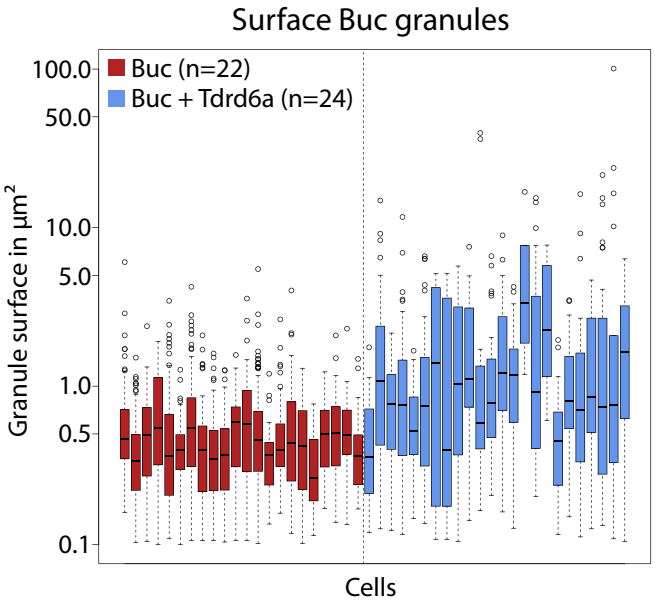

B

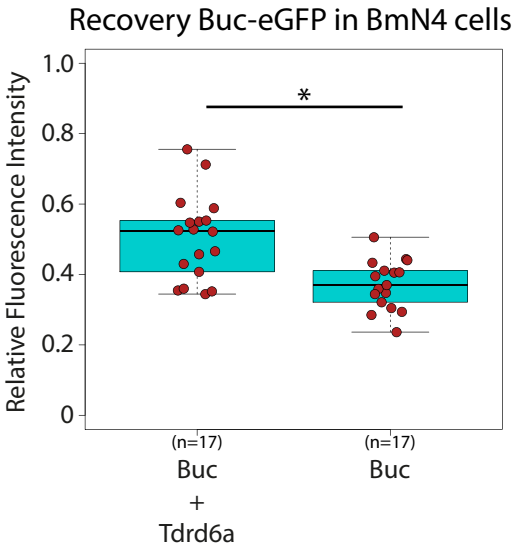

C

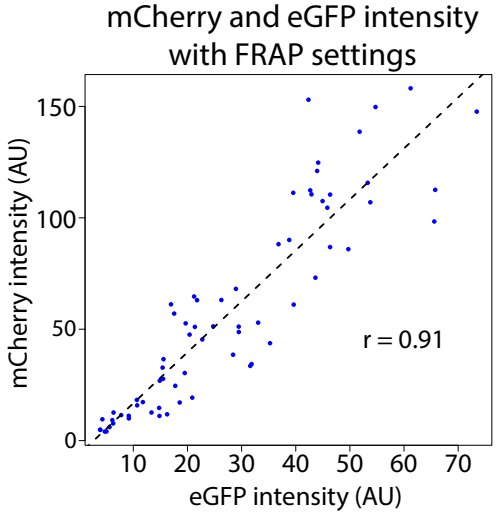

Supplemental Figure 7

A

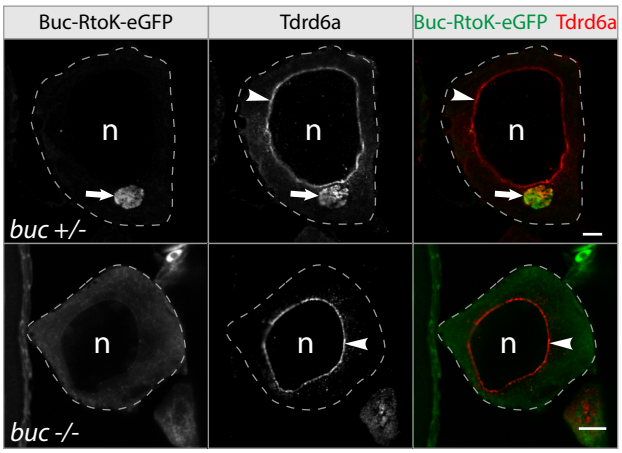

B

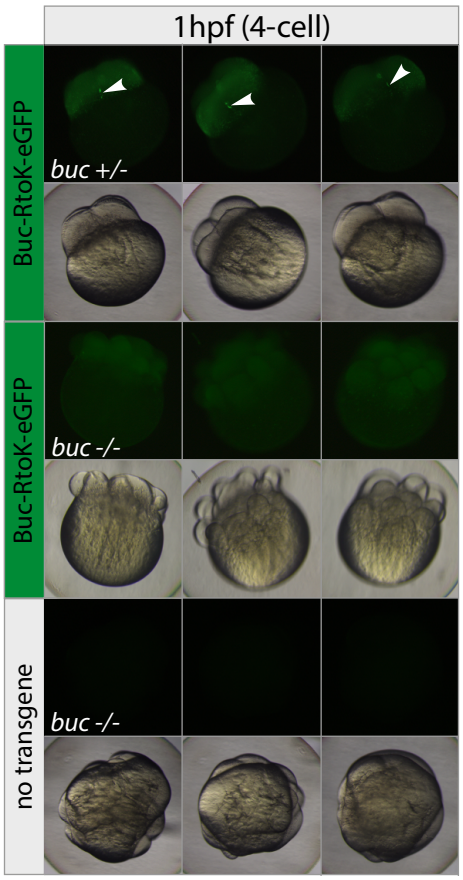

Supplemental Figure 1, Related to Figure 1. (A) Schematic overview of Tdrd6a. (B) RT-PCR of different tissues to confirm germline expression. (C) Tdrd6a co-localizes to Vasa-eGFP in nuage, to Buc-eGFP in the Bb (Riemer et al., 2015) and to Ziwi in the Gp. A Tdrd6a-mCherry-polyA3'UTR was used under a Ziwi promoter, which expresses until ~stage II oocytes. Scale bars (top-middle-bottom): 2µm, 10µm and 100µm (D) Western blot for Tdrd6a in wt and *tdrd6a-/-* ovary and testis. (E) Tdrd6a staining in wt and *tdrd6a* mutant ovary. Tdrd6a is lost from nuage in the *tdrd6a* mutant (arrowhead) but some signal from the Bb remains (arrow). Wt is taken along from Figure 1A for comparison. Scale bars indicate 10µm (F) Tdrd6a staining in wt and a MZ *tdrd6a* mutant 4-cell stage embryo. Arrowheads indicate the cleavage planes. Wt is taken along from Figure 1B for comparison. Scale bars indicate 100µm.

Supplemental Figure 2, Related to Figure 1. (A) Quantitative Western blot for Tdrd6a, Tdrd1 and IgG IPs (based on IRDye detection with LI-COR). Ziwi is 3.3x more present in Tdrd6a IPs compared to Tdrd1 IPs, when normalized to Zili. (B) Length distribution sRNA reads mapping to TEs for *tdrd6a+/-* and *tdrd6a-/-* ovary, as indicated. (C) 5' overlap of piRNAs in *tdrd6a+/-* and *tdrd6a-/-* ovary. Ping-pong Z-scores are 39 and 41 for *tdrd6a +/-* and *tdrd6a -/-* respectively. (D) 5' nucleotide bias displaying the typical 5'U bias in both genotypes. (E) The sense/antisense bias observed in ovary of *tdrd6a+/-* and *tdrd6a-/-* siblings is plotted for all DNA and RNA transposons. *Tdrd6a -/-* ovary shows a reduction in antisense piRNAs ($p = 0.03$) mapping to RNA elements. (F) Length distribution sRNA reads mapping to TEs for *tdrd6a+/-* and *tdrd6a-/-* early and late oocytes, as indicated. (G) 5' overlap of piRNAs in *tdrd6a+/-* and *tdrd6a-/-* early and late oocytes. Ping-pong Z-scores are 30 and

32 in early oocytes and 32 and 33 in late oocytes, for *tdrd6a+/-* and *tdrd6a -/-* respectively. (H) 5' nucleotide bias displaying an unaffected 5'U bias. (I,J) The sense/antisense bias observed in ovary of *tdrd6a+/-* and *tdrd6a-/-* siblings plotted for reads mapping against DNA and RNA transposons, early versus late (I) and *tdrd6a +/-* versus *tdrd6a -/-* (* indicates $p < 0.01$, Mann-Whitney-Wilcoxon Test) (J) RPM = Reads per million.

Supplemental Figure 3, Related to Figure 2. (A) Barplot displaying the number of cells per genotype and developmental timepoint used in this study. (B and C) t-SNE maps showing transcript counts of *nanog* and the *rps* gene group, respectively. (D) Barplot displaying the significance of enrichment for the different genotype-developmental time combinations in the six clusters identified in (2B). (E) Barplot displaying the RPKM counts for six Gp mRNAs from bulk RNA-seq of 1-cell stage wt and Mmut *tdrd6a* embryos, as indicated. Error bars indicate standard deviation obtained from three biological replicates. (F) Scatterplot displaying transcript counts in wt and Mmut PGCs at 3.5hpf based on scRNA-seq. Genes highlighted in red are 2 fold up or down regulated between genotypes with a p-value < 0.01 (p-value is calculated by negative binominal statistics and corrected for multiple testing (Benjamini–Hochberg)). (G) Barplot representing the Spearman correlation between Gp-Gp transcript and BG-BG transcripts in 3.5hpf old embryos, as indicated. Standard deviations of the Gp-Gp correlations were obtained by bootstrapping. (H) Tdrd6a RIP-qPCR analysis for *nanos3*, *dazl* and *vasa*. Enrichments were calculated compared to beads only RIP and normalized to *β-actin*. Error bars represent standard deviation of two biological replicates (* indicates p-value < 0.001, p-value obtained by two-sided Student's t-test). (I, J) Boxplots displaying the *hook2*-Gp and BG-BG correlations in 3.5hpf PGCs form wt and Mmut embryos, as indicated (* = p-value < 0.001, n.s. = non-significant, calculated by Wilcoxon test). (K) Ziwi

RIP-qPCR analysis for *nanos3*, *dazl* and *vasa*. Enrichments were calculated compared to beads only RIP and normalized to *β-actin*. Error bars represent standard deviation of two biological replicates (* = p-value < 0.05, p-value obtained by two-sided Student's t-test). (L) Western blot control for successful IP of (K).

Supplemental Figure 4, Related to Figure 3. (A, B) Additional electron micrographs to further illustrate *tdrd6a* heterozygous (A) and mutant (B) Balbiani bodies, including the Bbs from Figure 3E and F (bottom row). Overlays in the right panel indicate the Gp regions (yellow) and mitochondria (cyan) that can be appreciated in the middle panel.

Supplemental Figure 5, Related to Figure 4. (A) FISH against *nanos3* using anti-DIG IHC combined with Tdrd6a IHC visualizing Gp at a 4-cell stage embryo cleavage plane. (B) Maximum projections of Z-stacks of wt and Mmut Gp of 4-cell stage Buc-eGFP signals, used to calculate Gp volumes of Figure 4C. Red dotted line indicates the largest Gp fragment, of which the volume in in μm^3 was measured. Scalebars represent 5µm (A) and 10µm (B).

Supplemental Figure 6, Related to Figure 6. (A) Surface calculation of Buc-containing granules in transfected BmN4 cells in μm^2. Overall, granules increase in size in the presence of Tdrd6a, with large variation between co-transfected cells. (B) Boxplot of the recovery of separate FRAP experiments of Buc-eGFP as in Figure 6E, based on the average intensity value of the last 20 frames (* indicates p-value < 0.05, calculated by Wilcoxon test). (C) Fluorescence intensity of an mCherry-eGFP fusion construct as indicated, using the FRAP settings used in Figure 6E.

Supplemental Figure 7, Related to Figure 7. (A) Tdrd6a localization in sections of *buc+/-* and *buc-/-* oocytes in the Buc-RtoK-eGFP background. Arrow: Bb, arrowheads: nuage. Scale bar represents 10μm (B) Examples of 4-cell stage embryos of *buc +/-* and *-/-* mothers, with and without Buc-RtoK-eGFP. Without the presence of wt Buc, Buc-RtoK can rescue the lack of polarity of the *buc* phenotype (*buc -/-*, no transgene), even though most embryos display severe developmental defects (*buc -/-*, Buc-RtoK-eGFP). Arrowheads: Gp.